Ice melt influence on summertime net community production along the Western Antarctic Peninsula

R. Eveleth[a], N. Cassar[a], R.M. Sherrell[bc], H. Ducklow[d], M.P. Meredith[e], H.J. Venables[e], Y. Lin[a], Z. Li[a]

[a]Division of Earth and Ocean Sciences, Nicholas School of the Environment, Duke University, Durham, North Carolina, USA.

[b]Department of Marine and Coastal Sciences, Rutgers University, New Brunswick, New Jersey 08901, USA

[c]Department of Earth and Planetary Sciences, Rutgers University, Piscataway, NJ, 08854, USA.

[d] Lamont Doherty Earth Observatory, Columbia University, Palisades, NY 10964, USA

[e] British Antarctic Survey, Cambridge, CB3 0ET, United Kingdom

Corresponding author: R. Eveleth, Old Chemistry Bldg., Duke University, EOS, Box 90227, Durham, NC 27708 (rachel.eveleth@duke.edu)

Abstract

The Western Antarctic Peninsula (WAP) is a highly productive marine environment that is undergoing rapid change, with consequences for productivity and total ecosystem carbon cycling. We present continuous underway O_2/Ar estimates of net community production (NCP_{O2Ar}) in austral summer 2012, 2013 and 2014 at sub-kilometer horizontal resolution within the Palmer Long-Term Ecological Research (Pal-LTER) grid region of the WAP. Substantial spatial variability is observed with NCP_{O2Ar} ranging from 0 to 790 mmol O_2 m^{-2} d^{-1} and considerable interannual variability with mean values in the grid region of 54.4 ± 48.5, 44.6 ± 40.5, and 85.6 ± 75.9 mmol O_2 m^{-2} d^{-1} in 2012, 2013 and 2014 respectively. Based on a strong correlation (r^2=0.83) between residence time integrated NCP_{O2Ar} and NCP_{DIC} derived from seasonal DIC drawdown, we find the observed NCP_{O2Ar} spatial and interannual variability to be consistent with the December-January NCP_{DIC} magnitude. Seeking to explain the mechanistic drivers of NCP in the WAP, we observe a linear relationship between NCP_{O2Ar} and meteoric water content derived from $\delta^{18}O$ and salinity. This correlation may be due to Fe supply from glacial melt and/or strengthening of stratification and relief of light limitation. Elevated surface Fe availability, as indicated by Fv/Fm and measurements of surface water dissolved Fe and Mn (a rough proxy for recent potential Fe availability), and shallower, more stable mixed layers are present where meteoric water and/or sea ice melt is high near the coast. Light limitation is evident in the WAP when mixed layer depths are greater than ~40 m. Additionally we document hotspots of NCP associated with submarine canyons along the WAP. While it is difficult to predict how the physical-biological system might evolve under changing climatic conditions, it is evident that NCP, and potentially carbon flux out of the mixed layer, along the WAP will be sensitive to shifts in meltwater input and timing.

1. Introduction

The climate of the Western Antarctic Peninsula (WAP) is changing rapidly, with July air temperatures increasing 6.3°C since 1951 [*Ducklow et al*., 2007], sea ice duration decreasing by approximately 3 days each year [*Stammerjohn et al*., 2008], retreat of the majority of glaciers [*Vaughan*, 2006] and shifting ecological structures [*Ducklow et al*., 2013; *Montes-Hugo et al*., 2009]. With such pronounced climatic changes we would likely expect accompanying impacts on net community production (NCP, gross photosynthesis minus community respiration) and regional carbon export production that could in turn feed back on the climate and ecosystem.

Predictive skill requires mechanistic understanding of the controlling processes. Since 1993, primary production has been estimated discretely in the WAP region as part of the Palmer Long-Term Ecological Research (Pal-LTER) program [*Ducklow et al*., 2013]. These previous studies have broadly identified water column stability (thus light) and Fe supply as the likely main controls on primary production in the WAP [*Dierssen et al*., 2002; *Ducklow et al*., 2007; *Smith et al*., 1998; *Vernet et al*., 2008] consistent with other seasonal ice zones in the Southern Ocean, however no Fe measurements were available in the region prior to our study. The physical environment of the Pal-LTER study region is diverse, including offshore (northwest of the shelf break), shelf and coastal zones, deep glacially-scoured canyons that act as conduits of heat and nutrients via deep water intrusions onto the shelf, and pronounced latitudinal gradients. Across this varied seascape we might expect the relative importance of light and Fe limitation to change, yet currently this variability is not well understood. Additionally, the physical underpinnings of seasonal stratification and Fe supply including sea ice, winds, horizontal and vertical advection and mixing, and freshwater supply are complex and poorly resolved.

65 Few studies have documented NCP in the WAP, hence little is known about its
66 magnitude, interannual variability, spatial variability and drivers. *Huang et al*. [2012] presented
67 O_2/Ar-based NCP measurements in the Pal-LTER study region and found evidence of Fe and
68 light limitation. Consistent with the prior discrete incubation NCP studies in the WAP [*Carrillo*
69 *et al*., 2004], they document declining NCP with increasing distance from shore consistent with
70 onshore-offshore gradients in primary production but, limited to only 46 discrete observations,
71 could not resolve variability embedded within this gradient. *Tortell et al*. [2014] captured
72 continuous time series of the pCO_2 and O_2/Ar spring-summer seasonal cycle at Palmer Station
73 that showed a seasonal progression closely tied to water column stability and mixed layer depth.
74 This well-resolved seasonal cycle provides a valuable context for broad-scale spatial surveys,
75 such as presented here, but does not inform our understanding of variability across the WAP
76 region. Recently, *Tortell et al*. [2015] presented underway O_2/Ar measurements in the Pal-LTER
77 grid region in the austral summer 2011. Here we resolve additional interannual variability with
78 three years of spatial surveys.
79 Three years of summertime high spatial resolution (<1 km) underway NCP data along the
80 WAP are presented. We estimate NCP from Equilibrator Inlet Mass Spectrometry (EIMS)
81 measured O_2/Ar (NCP_{O2Ar}) and NCP from underway pCO_2 (NCP_{DIC}) and use their relationship to
82 elucidate the January contribution of NCP to the elapsed growing season. In a companion paper
83 (Eveleth *et al*., in review b, this issue) we show that biological processes primarily control O_2
84 and pCO_2 in the WAP and that there is substantial mesoscale horizontal variability across the
85 region. Here we seek to explain which underlying mechanisms are setting this biological
86 variability, with a focus on glacial and sea-ice melt water influences.
87

2. Methods

Data presented here were collected in January-February 2012, 2013 and 2014 onboard the ARSV Laurence M Gould in conjunction with the Pal-LTER annual cruises. The Pal-LTER sampling scheme spans a ~700 km x 250 km grid with discrete surface sampling every 20 km along 100 km spaced grid lines (Fig. 1). Conductivity-temperature-depth (CTD) casts were conducted at selected stations every 40-100 km with a SeaBird 911plus instrument (temperature sensor model 3plus with accuracy ±0.001ºC, conductivity sensor model 4C with accuracy ± 0.002 S/m). Mixed layer depth (MLD) was determined as the depth at which the potential density increased 0.125 kg m^{-3} relative to the surface value [*Monterey and Levitus*, 1997]. Photochemical efficiency of photosystem II (Fv/Fm) measurements were taken discretely with a fluorescence induction relaxation system (FIRe) following standard published protocol [*Gorbunov et al*., 1999]. Raw surface values have been re-calibrated to account for sampling artifacts using FPRO2 (Max Gorbunov, 2015, personal communication) but should still be treated as qualitative. Some variability in Fv/Fm may be due to diel cycles but we discuss all data here. We do not observe any relationship between time of day or surface irradiance and Fv/Fm (Fig. S1), indicating that the spatial variability may be overwhelming the diurnal cycle. We do additionally show a subset of nighttime Fv/Fm data from the expected peak window of photochemical efficiency defined here as between midnight and 4 am [*Huang et al*., 2012]. Sea surface salinity and temperature (SSS and SST respectively) here refer to two-minute averages of these properties measured continuously in the ship's underway seawater supply by a flow-through thermosalinograph (SBE 45 MicroTSG accuracy ± 0.0003 S/m, ±0.002ºC, intake at 5 m depth). Gases (O_2/Ar and pCO_2) were also measured underway. Continuous (2-min averaged) underway O_2/Ar measurements were performed using Equilibrator Inlet Mass Spectrometry

(EIMS) [*Cassar et al*., 2009] (method also detailed in companion paper [Eveleth *et al*., in review b, this issue]). In this method, gasses are equilibrated from seawater flowing through the ship's underway lines using a gas permeable membrane contactor cartridge, and the ratio of O_2 to Ar is analyzed using a quadrupole mass spectrometer (Pfeiffer Prisma model QMG 220 M1). Seawater samples are calibrated against the stable atmospheric O_2/Ar ratio every four hours. The instrument precision is ±0.3%. Respiration in the ship's seawater lines is likely negligible as *Juranek et al*. [2010] show that respiration is slow at low temperatures (0.5%) and water residence time in the lines is ~1 minute. Sink and Niskin bottle comparisons were performed using potentiometric Winkler titrations in January, 2016. The data show no significant difference between the underway lines of the LMG and Niskin bottles closed at the surface (0.06%, n=9). Surface pCO_2 (pCO_{2meas}) was measured every 2.5 minutes (the approximate integration time of the equilibration system) using a 30 L shower-type air-water equilibrator and an IR CO_2 analyzer [*Munro et al*., 2015]. Underway data were time matched to station data, as an average of all data measured within 15 minutes of discrete sampling.

Surface chlorophyll concentration was measured ~weekly from ~November-March at Station B and E near Palmer Station and from ~October-May at the British Antarctic Survey's Rothera Research Station's oceanographic and biological time series site (RaTS) as described in *Saba et al*. [2014] and *Clarke et al*. [2008] respectively (station locations indicated on Fig. 1). Chlorophyll a concentration was also measured discretely on the cruise track. Seawater samples were filtered and extracted in 90% acetone, frozen and stored for 24 hours, then measured using a digital Turner Designs fluorometer following standard protocol [*Smith et al*., 1981].

2.1 Fe and Mn Concentration

Surface water was collected for trace metal analysis during the January 2012 expedition, using a non-contaminating towfish deployed from a laterally-extended crane off the starboard side of the ship, avoiding contamination from the ship's hull. Seawater was pumped through an acid-cleaned plastic tube, attached to the fish and collecting water at ~2 m depth, to a HEPA-filtered clean lab built within the ship's main science lab, where it was filtered at 0.2 μm through acid-cleaned capsule filters (Acropak 200, Pall®). The surfaces contacted by seawater in this system were Teflon, polypropylene, polyethylene and polyethersulfone only. Filtered water samples in acid-cleaned low density polyethylene bottles (Nalgene) were acidified at sea to pH ~2.0 using ultraclean HCl (Fisher Optima HCl, concentration in seawater 0.012 M) in order to prevent adsorptive loss of metals to container walls and to prevent biological growth. Seawater samples were analyzed at Rutgers University for dissolved Fe and Mn (in addition to Zn, Cu and Ni; reported elsewhere) using an automated flow injection ICP-MS method developed in R. Sherrell's laboratory [*Lagerström et al*., 2013]. Briefly, the automated device loaded a 9 mL aliquot of seawater, buffered online to pH 7.0 with 3 mL of acetic acid/ammonium hydroxide buffer, onto a column packed with Nobias PA1 chelating resin (Hitachi High-Technologies). The column was eluted with 1.5 M nitric acid directly into the nebulizer of an Element-1 sector field ICP-MS (Thermo-Finnigan, Bremen, Germany). The eluate, a 200-fold concentrate of the sample but with greatly reduced major ion concentration, was analyzed in medium resolution and temporal peak integration was performed using custom software coded in Matlab. Quantification was carried out using internal isotope dilution (Fe) for each sample or matrix matched external standards in seawater (Mn), the latter preconcentrated through the chelating column at the beginning and end of each analytical session, and corrected for instrumental sensitivity drift.

156 Analytical duplicates were measured every sixth sample and typically displayed 1–3%
157 deviation about the mean. The long-term precision over many analytical runs over a period of
158 months, as demonstrated by repeated analysis of a large-volume in-house seawater standard from
159 the Ross Sea (analyzed 5–6 times during each analytical session), was 3% for Fe (RSD; see
160 Table 3 in *Lagerström et al*. [2013]). Accuracy was verified by repeated analysis of reference
161 seawater materials (SAFe S and D2, GEOTRACES S and D), which showed agreement within
162 one standard deviation of the consensus values for almost all reference seawaters (see Table 5 in
163 *Lagerström et al*. [2013]).
164 Methods for the collection and analysis of particulate Fe (pFe) followed *Planquette and*
165 *Sherrell* [2012]. Briefly, particles were filtered from towfish-collected seawater onto 0.45 μm
166 pore size filters (Supor; Pall®) within the shipboard clean lab. Filters were then frozen for
167 shipping and subjected to complete acid digestion in nitric and hydrofluoric acid, followed by
168 analysis by ICP-MS at Rutgers University.
169
170 **2.2 $\delta^{18}O$ Freshwater Fraction Determination**
171 Discrete sampling for the ratio of stable isotopes of oxygen in seawater ($\delta^{18}O$) was
172 conducted from the underway water supply at 5 m depth on the Pal-LTER cruises. Additionally,
173 samples were drawn from Niskin bottles closed at various depths during the station-based CTD
174 profiling on the cruises. Samples were collected in 50 ml glass vials that were sealed with
175 stoppers and aluminum crimps, and were transported by dark cool stow to the Natural
176 Environment Research Council Isotope Geochemistry Laboratory (NIGL) at the British
177 Geological Survey, U.K., for analysis using the equilibration method for oxygen [*Epstein and*
178 *Mayeda*, 1953]. Samples were run on a VG Isoprep 18 and SIRA 10 mass spectrometer, with

179 random duplicates indicating a precision better than ±0.02 ‰ was attained. To obtain
180 quantitative details on the freshwater sources from these data, they were used alongside salinity
181 in a simple 3-endmember mass balance, whereby each water sample is presumed to be a three
182 component mixture of CDW, sea ice melt and meteoric water, and the relative proportions of
183 each derived. We use end-member salinity and $\delta^{18}O$ values of 34.73 and 0.1‰ respectively for
184 CDW, 7 and +2.1‰ for sea ice melt and 0 and -16‰ for meteoric water. Full details of the
185 methodology are given in *Meredith et al*. [2013].
186
187 **2.3 NCP_{O2Ar}**
188 Neglecting vertical mixing, the net biological oxygen flux is a function of the net
189 community production (NCP) and gas exchange of biologically-produced oxygen ($[O_2]_{bio}$) with
190 the atmosphere [*Cassar et al*., 2011]

191 $$MLD\frac{d[O_2]_{bio}}{dt} = NCP_{O2Ar} - k_{O2}[O_2]_{bio} \quad (1)$$

192 where k_{O2} is the piston velocity (m d^{-1}), and

193 $$[O_2]_{bio} = [O_2]_{total} - [O_2]_{phys} \approx \frac{[Ar]}{[Ar]_{sat}}[O_2]_{sat}\Delta(O_2/Ar) \quad (2)$$

194 In steady state, NCP_{O2Ar} (mmol O_2 m^{-2} d^{-1}) in the mixed layer over the residence time of oxygen
195 (~10 days in this region) is commonly approximated by

196 $$NCP_{O2Ar} \approx k_{O2}[O_2]_{sat}\Delta(O_2/Ar) \quad (3)$$

197 where

198 $$\Delta(O_2/Ar) = \left[\frac{([O_2]/[Ar])_{meas}}{([O_2]/[Ar])_{sat}} - 1\right]. \quad (4)$$

199 $([O_2]/[Ar])_{meas}$ is the measured O_2/Ar ratio from EIMS. The equilibrium saturation
200 concentrations of O_2 ($[O_2]_{sat}$) and Ar ($[Ar]_{sat}$) were calculated using underway temperature and
201 salinity measurements and the equations of Garcia and Gordon [1992] and Hamme and Emerson

202 [2004] respectively. In this region, O_2 is often undersaturated below the mixed layer. Negative
203 NCP_{O2Ar} could reflect surface heterotrophy, or vertical mixing of oxygen-undersaturated waters.
204 In regions where vertical mixing is significant, NCP_{O2Ar} represents a lower bound on true NCP.
205 [*Cassar et al*., 2014], but here we assume that negative O_2/Ar supersaturation (and thus negative
206 NCP_{O2Ar}) values are contaminated by vertical mixing and remove them (~10% of sampled
207 points) from our NCP analysis and treat NCP_{O2Ar} as a conservative estimate of NCP magnitude
208 [*Cassar et al*., 2007; *Giesbrecht et al*., 2012; *Reuer et al*., 2007]. The approximation of NCP_{O2Ar}
209 assumes that $[Ar]/[Ar]_{sat}$ equals unity. By making this assumption we are introducing an error in
210 NCP_{O2Ar} that is equal to the observed Ar saturation. This is an important note for calculations of
211 NCP_{O2Ar} when Ar concentration deviates substantially from the equilibrium saturation
212 concentration [*Eveleth et al*., 2014] (e.g. brine where Ar undersaturation may be as low as 45%
213 [*Top et al*., 1988]). Argon supersaturation ranged from -5.3% to 2.8% in 2012 in the WAP, as is
214 explored in the companion paper [Eveleth *et al*., in review b, this issue]. Under these conditions,
215 the error associated with this assumption is negligible compared to the error in wind speed
216 parameterization of the piston velocity (~40%) [*Bender et al*., 2011]. We estimate piston velocity
217 using four-times daily NCEP/NCAR reanalysis wind speed and the parameterization of
218 *Wanninkhof* [1992]. Piston velocity is weighted as in *Reuer et al*. [2007] to account for wind
219 speed history prior to sampling.

220 Sufficient time series measurements of dissolved organic carbon (DOC) across the grid
221 are not available to assess accumulation in the mixed layer. NCP is commonly taken to estimate
222 carbon export from the mixed layer in the Southern Ocean where DOC in the mixed layer is low
223 relative to the observed NCP rates [e.g. *Allison et al*., 2010; *Carlson et al*., 2002; *Hansell and*
224 *Carlson*, 1998; *Ishii et al*., 2002; *Sweeney et al*., 2000], as specifically shown in the WAP by

225 *Huang et al*. [2012]. However if significant dissolved or particulate organic carbon accumulation
226 did occur, NCP_{O2Ar} would overestimate carbon flux out of the mixed layer [*Sweeney et al*.,
227 2000].
228
229 **2.4 NCP_{DIC}**
230 DIC was determined from pCO_2, salinity-based total alkalinity (TA) estimates, and
231 underway temperature, salinity and pressure using CO2SYS [*van Heuven et al*., 2011] and
232 dissociation constants for carbonic acid by *Lueker et al*. [2000] and for boric acid by *Dickson*
233 [1990]. The following salinity-TA algorithm for the LTER grid region was determined by *Hauri*
234 *et al*. [2015] from linear least squares fits of historical discrete surface measurements of
235 alkalinity and salinity from 1993-2013:
236 $TA_{LTER} = 58.5*S + 322.1$ [*Hauri et al*., 2015] (5)
237 TA_{LTER} has a root mean square error (RMSE) of 16.8 μeq kg^{-1} [*Hauri et al*., 2015]. Salinity-
238 predicted TA appears to underestimate TA by as much as 25 μeq kg^{-1} in the northern portion of
239 the Pal-LTER grid region, as seen by comparison with discrete TA measurements in 2012 (Fig.
240 S2a). This leads to a local DIC underestimation of up to 50 μmol kg^{-1} (root mean squared error
241 ±15.21 μmol kg^{-1} (~0.7%), Fig. S2b). Discrete measurements are not available for comparison in
242 2013 and 2014. DIC was salinity normalized (nDIC) to 35 to account for dilution by meteoric
243 water and sea-ice meltwater input.
244 Average winter DIC in the WAP was calculated from a climatology of all winter (June-
245 August) underway pCO2 and salinity measurements between 1998-2013
246 (http://www.ldeo.columbia.edu/res/pi/CO2/). Winter pCO2 does not show any significant long-
247 term trend over this time [*Hauri et al*., 2015]. We calculated nDIC the same way as for the

summer months. Mean winter nDIC was 2272 ± 8 μmol kg^{-1} (SE 0.04 μmol kg^{-1}). While there is some regional variability across the grid, data were too sparse to resolve a spatial climatology.

The seasonal mixed layer integrated NCP rate (mmol C m^{-2} d^{-1}) can be calculated from the DIC drawdown as follows:

$$NCP_{DIC} = \frac{(nDIC_w \cdot \rho_w - nDIC_s \cdot \rho_s) \cdot MLD}{\Delta t} \quad (6)$$

where $nDIC_w$ is the mean winter nDIC (2272 μmol kg^{-1}), $nDIC_s$ is the summer value derived from pCO_2 measured in this study, ρ_w and ρ_s are the prescribed winter (-1.85°C; 33.88 [*Martinson et al*., 2008]) and measured summer water densities respectively, MLD (m) is the mixed layer depth from the nearest CTD cast, and Δt is the length of the growing season in days. The length of the growing season could be approximated from satellite chlorophyll data, relative sea-ice retreat timing or in situ Chl a time series records at Palmer Station and Rothera Station (Fig. 2), but is not required here as we present growing season integrated NCP_{DIC} (see Section 3.2). Very likely, MLDs shoaled during the growing season, but because of a lack of December data across the grid region we use the measured January MLD. This probably leads to an underestimation of NCP_{DIC} but significant primary production likely does not occur until after mixed layer shoaling [*Tortell et al*., 2014; *Venables et al*., 2013]. Additional uncertainties as they relate to the data interpretation are discussed in section 3.2.

3. Results and Discussion

3.1 NCP_{O2Ar}

NCP_{O2Ar} in the Pal-LTER grid of the WAP (Fig. 3) averaged 54.4 ± 48.5 mmol O_2 m^{-2} d^{-1} in 2012, 44.6 ± 40.5 mmol O_2 m^{-2} d^{-1} in 2013 and 85.6 ± 75.9 mmol O_2 m^{-2} d^{-1} in 2014, neglecting negative values and noting that spatial surveys in each year vary so full-grid

averaging could be biased by the cruise track. Means by sub-region are presented in Fig. 4 with offshore, southern onshore and northern onshore regions roughly dividing the shelf and coast from the slope and latitudinally separating regions known to have hydrographic, sea ice and other biological distinctions [*Bernard et al*., 2012; *Martinson et al*., 2008; *Stammerjohn et al*., 2008; *Steinberg et al*., 2015] but these sub-regions cannot fully resolve the gradients in observations. If we consider only a subset of stations (those which were occupied in all three years), NCP_{O2Ar} averaged 37.3 ± 28.5 mmol O_2 m^{-2} d^{-1} in 2012, 12.3 ± 17.5 mmol O_2 m^{-2} d^{-1} in 2013 and 50.8 ± 63.0 mmol O_2 m^{-2} d^{-1} in 2014, consistent with the interannual variability documented in full grid averages. The interannual variability in *in situ* observations clearly shown in Fig. 3 is also supported by mean January satellite NCP estimates in the grid region, with 2014 being anomalously productive. Satellite NCP estimates were derived from a WAP specific satellite Chl algorithm and *in situ* comparisons of NCP_{O2Ar} and Chl concentration from 2008-2014 (Li *et al*., in review). There is relatively high production near the coast, decreasing offshore in all years (Figs. 3, 4). In addition to the higher overall magnitude, NCP in the onshore region (including shelf and coastal regions roughly defined as east of grid station 100 (Fig. 3)) is also more spatially variable than offshore (Eveleth *et al*., in review b, this issue). This onshore-offshore trend is consistent with previous studies of NCP [*Huang et al*., 2012], chlorophyll and primary production [*Garibotti et al*., 2005; *Smith et al*., 1998; *Vernet et al*., 2008] and bacterial activity [*Ducklow et al*., 2012].

We also noted negative biological O_2 flux (NCP_{O2Ar} estimates including negative values) in the coastal straits north of the traditional Pal-LTER sampling region (Fig. S3), specifically persistent negative $\Delta O_2/Ar$ in the Gerlache Strait in all crossings save one in 2014. While it is possible that this area is net heterotrophic in the summer, the values could alternatively be

exposing a limitation of our methodology. We assume that there is no vertical mixing across the lower mixed layer interface, however the Gerlache Strait and adjacent inner bays have been shown to be strongly influenced by upwelling of modified upper CDW (UCDW) routed through the strait via a deep canyon [*Espinasse et al*., 2012]. Upwelling would bring O_2-undersaturated water to the surface, influencing our NCP estimation. Modified UCDW, possibly influenced by Fe inputs from shelf sediments [*Sherrell et al*., 2015], may also be a source of Fe in the region, so this upwelling may promote high NCP. The Gerlache Strait and surrounding inner bays have been shown to be significantly productive in the summer (carbon fluxes up to 800 mg C m^{-2} d^{-1} [*Anadon et al*., 2002; *Karl*, 1991]), supporting extremely high krill and whale density in the austral fall [*Nowacek et al*., 2011]. In February 2014 (Fig. S3), there was a very large bloom in the Gerlache Strait with NCP_{O2Ar} reaching ~175 mmol O_2 m^{-2} d^{-1}, ~20 days after the region was O_2/Ar undersaturated, giving support to the prominent role of upwelling controlled productivity in the straits. Unfortunately, this area is outside of the traditional Pal-LTER sampling grid, thus we have no depth information and are limited in our ability to further explain our $\Delta(O_2/Ar)$ observations. The following analysis will first explore the validity of the O_2/Ar-based NCP measurements in the grid region and then attempt to develop a mechanistic understanding of the onshore-offshore NCP gradient and coastal hot spots, especially as they relate to meltwater input. Negative NCP_{O2Ar} values are not considered in the remainder of the discussion, as they may be reflective of upwelling processes rather than net heterotrophy.

3.2 Biological Oxygen and DIC Inventories

NCP_{O2Ar} has a memory of production over the relatively short ~10 day residence time of O_2 in the mixed layer. This short residence time makes it difficult to discriminate between spatial

317 and temporal variability when interpreting observed O_2/Ar signals alone. For example, high
318 NCP_{O2Ar} in a particular location could indicate a region of persistently high productivity or our
319 sampling time might have simply coincided with the peak of a short lived bloom in that location.
320 Further, interannual variability in NCP_{O2Ar} may reflect variability in overall summer NCP
321 magnitude, or instead a shifting phenology relative to sampling date, for example in the far south
322 where we encounter ice-edge blooms in some years but miss them in others. We employ
323 estimates of recent and seasonal organic carbon production from NCP_{O2Ar} and NCP_{DIC}
324 respectively to investigate these issues as well as to corroborate our NCP_{O2Ar} estimates with an
325 independent measurement. This approach builds on *Carrillo et al*. [2004] and *Tortell et al*.
326 [2015] in the WAP, as well as the discussion of O_2 and CO_2 gas fluxes presented in the
327 companion paper (Eveleth *et al*., in review b, this issue). In order to properly assess timing and
328 the biologically-driven relationship between O_2 and CO_2 we need to isolate the biological
329 components (e.g. utilizing Ar in conjunction with O_2 and salinity normalizing derived DIC) and
330 compare time-integrated inventories rather than fluxes.
331 To obtain a mixed layer inventory of biological oxygen we integrate Equation (1) with
332 respect to time and multiply by MLD to obtain

333 $$\mathrm{MLD}[O_2]_{\mathrm{bio}(t)} = \mathrm{MLD}\frac{\mathrm{NCP_{O2Ar}}}{k_{O2}} + \mathrm{MLD}\cdot \mathrm{Ce}^{-\frac{k_{O2}}{\mathrm{MLD}}t} \quad (7)$$

334 where C is an arbitrary constant of integration. Thus, under steady-state conditions

335 $$\mathrm{MLD}[O_2]_{\mathrm{bio}(\infty)} = \tau_{O2}\mathrm{NCP_{O2Ar}}\,. \quad (8)$$

336
337 Converting to carbon units using a stoichiometric C/O_2 of 1:1.4 [*Laws*, 1991], we obtain the
338 mixed layer organic carbon production inventory (mmol C m^{-2}) during τ_{O2}, the residence time of
339 O_2 in the mixed layer (~10 days). The growing season carbon production (mmol C m^{-2}) is
340 approximated by

$$\int_0^t \mathrm{NCP}_{\mathrm{DIC}} \approx \Delta t\ \mathrm{NCP}_{\mathrm{DIC}} = (\mathrm{nDIC}_{\mathrm{w}} \cdot \rho_{\mathrm{w}} - \mathrm{nDIC}_{\mathrm{s}} \cdot \rho_{\mathrm{s}}) \cdot \mathrm{MLD}. \quad (9)$$

where Δt is the length of the growing season and $\mathrm{NCP}_{\mathrm{DIC}}$ is as given in Equation 6. This is equivalent to a mixed layer inventory of seasonal biological DIC drawdown independent of the length of the growing season. NCP_{DIC} represents seasonal biological carbon drawdown here because the residence time of pCO_2 in the mixed layer is months to years. Our tentative estimate for the uncertainty in the seasonal biological DIC drawdown, adding uncertainties in quadrature, is ±8% not including any error associated with our use of the summer mixed layer depth here which may lead to significant underestimation of NCP_{DIC}.

The time-integrated NCP properties $\tau_{O2}\mathrm{NCP}_{\mathrm{O2Ar}}$ and $\Delta t\ \mathrm{NCP}_{\mathrm{DIC}}$ are highly correlated with a slope of 0.37 and an r^2 of 0.83 (Model II least squares bisector regression, $p<0.0001$, Fig. 5). If NCP does not change over the growing season (i.e. $NCP_{O2Ar} = NCP_{DIC}$), the slope of the regression should reflect the ratio of the residence time of O_2 at the ocean surface to the length of the growing season. The average τ_{O2} during this study was ~10 days (MLD/k_{O2}) and the length of the growing season Δt was ~30 days, as first ice retreat from the region was no more than 36 days before sampling and chlorophyll time series at Palmer Station and RaTS show bloom activity starting in late November-December (Fig. 2). Thus the slope of 0.37 is approximately what would be expected for the ratio of τ_{O2} to Δt. The slope may indicate that NCP_{O2Ar} and NCP_{DIC} are near equal and O_2/Ar estimates are capturing persistent December-January spatial variability in the WAP rather than reflecting the impact of short-lived blooms. However, we cannot rule out any other combination of $\tau_{O2}\mathrm{NCP}_{\mathrm{O2Ar}}$: $\Delta t\ \mathrm{NCP}_{\mathrm{DIC}}$ that leads to a ~1/3 ratio such as a longer growing season and higher recent NCP than the growing season average. Interestingly, all three years display the same relationship between $\tau_{O2}\mathrm{NCP}_{\mathrm{O2Ar}}$ and $\Delta t\ \mathrm{NCP}_{\mathrm{DIC}}$ (slope 0.36 ± 0.005, 0.36 ± 0.004, 0.37 ± 0.002 in 2012, 2013 and 2014, respectively),

suggesting that we are capturing interannual variability in December-January NCP magnitude with the O_2/Ar approach. Of course this correlation does not fully capture the full growing season's organic carbon production; chlorophyll concentration time series at Palmer Station (stations B and E) and RaTS as well as satellite data show that blooms occur until late March. In fact, based on the RaTS time series, chlorophyll concentration did not peak in Ryder Bay until March in 2012 and 2013 (Fig. 2). Li *et al*. (in review) use satellite derived NCP climatologies to show that in the productive onshore region of the WAP, peak annual NCP is observed in January.

It is possible that deviations from the observed $\tau_{O2}NCP_{O2Ar}$: $\Delta t\ NCP_{DIC}$ relationship could indicate local bloom timing since O_2/Ar re-equilibrates with the atmosphere much faster than pCO_2. $\tau_{O2}NCP_{O2Ar}$: $\Delta t\ NCP_{DIC}$ significantly less than 0.37 might indicate that the recent NCP rate captured with O_2/Ar is much lower than the rate earlier in the season (i.e. the peak bloom occurred prior to sampling) while a ratio much greater than 0.37 would indicate that the current rate is higher than the seasonal average and we are capturing a more recent bloom. We assessed the validity of the $\tau_{O2}NCP_{O2Ar}$: $\Delta t\ NCP_{DIC}$ ratio as a tracer of bloom timing by comparing it to satellite derived NCP (Li *et al*., in review) at the time of cruise sampling relative to NCP in the months prior. No clear relationship exists between $\tau_{O2}NCP_{O2Ar}$: $\Delta t\ NCP_{DIC}$ and $NCP_{sat\ 8\ day}$: $NCP_{sat\ 32\ day\ avg}$ (Fig. S4). Additionally we see no relationship between the difference between $\tau_{O2}NCP_{O2Ar}$ and $\Delta t\ NCP_{DIC}$ and the days of open water prior to sampling, which may be an indicator of bloom timing. Because of all the uncertainties discussed herein, scatter about the $\tau_{O2}/\Delta t$ slope is not a reliable indicator of bloom timing in the WAP. More likely, deviations from 0.37 could arise from limitations in both NCP estimation methods. Error in NCP_{DIC} may arise from errors in DIC reconstruction from pCO_2, horizontal and vertical transport, calcium

387 carbonate dissolution/precipitation, gas exchange (2-10% underestimation likely based on
388 *Sweeney et al*. [2000]) or by using an $nDIC_w$ climatology that does not represent true winter DIC
389 in a particular location or year. NCP from O_2/Ar may be biased due to vertical mixing, Ar
390 supersaturation, non-steady state conditions over the residence time of O_2, variability in piston
391 velocity (for example due to partial ice cover, which is not accounted for here) or a
392 stoichiometric C/O_2 different from 1:1.4. *Tortell et al*. [2014] suggest, for example, that the
393 WAP quotient may be closer to 1:1. Both NCP estimates would likely be biased low if vertical
394 mixing were significant, though the extent would likely differ depending on vertical gradients of
395 O_2 and DIC and the timing of the mixing. There may also be geographical variations in $\tau_{O2}/\Delta t$.
396 Additionally, it is important to note that this is inherently an Eulerian (not Lagrangian) study and
397 as a result of the differing residence times of O_2 and pCO_2, NCP_{O2Ar} and NCP_{DIC} are not
398 necessarily reflecting production in the same water parcel over time. NCP_{DIC} reflects larger
399 spatial and temporal footprints.
400 Given the multitude of uncertainties and assumptions, the strong correlation (r^2=0.83)
401 could be fortuitous (i.e. multiple factors canceling each other), or instead may indicate that those
402 factors are of second-order importance. If the latter is true, it notably implies that the
403 assumptions for estimating NCP based on O_2/Ar in this region are generally valid, although we
404 cannot rule out that they contribute to some of the noise around the regression. Two main
405 limitations of the O_2/Ar method are the necessary assumptions of insignificant vertical mixing
406 and steady-state conditions [*Cassar et al*., 2009; *Jonsson et al*., 2013]. *Cassar et al*. [2014]
407 recently showed that the influence of vertical mixing on biological oxygen can be addressed by
408 taking concurrent measurements of N_2O and using a composite "N_2O-O_2/Ar" tracer that is
409 conservative with respect to water mass obduction (any vertical mixing into the mixed layer

410 including upwelling, entrainment, and diapycnal mixing). Others have addressed the steady-state
411 assumptions with Lagrangian studies [*Hamme et al*., 2012]. Here we are able to indirectly assess
412 the steady-state assumption by comparing $\tau_{O2}NCP_{O2Ar}$ to $\Delta t\ NCP_{DIC}$. Such observations in other
413 regions may allow us to determine whether the large discrepancies between biological O_2 flux
414 and NCP in the modeling study of *Jonsson et al*. [2013] are significant.
415
416 **3.3 Drivers of NCP**
417 In the remainder of the discussion we refer to the O_2/Ar-derived mixed-layer integrated
418 NCP_{O2Ar} rates (mmol O_2 m^{-2} d^{-1}), with the understanding that these are broadly consistent with
419 December-January production rates and the timescale of NCP_{O2Ar} estimates are more relevant to
420 timescales of phytoplankton kinetics. NCP_{O2Ar} displays a significant linear correlation with
421 surface chlorophyll concentration (n=129, r^2=0.54 p<0.0001, Fig. 6) and gross primary
422 production [*Huang et al*., 2012]. With replete macronutrients [*Ducklow et al*., 2007; *Garibotti et*
423 *al*., 2005; *Huang et al*., 2012], the primary candidates for bottom-up control on NCP_{O2Ar} are light
424 and iron. While the following discussion focuses on physical drivers it is important to note that
425 top-down controls on primary production likely also have significant influences on NCP_{O2Ar}. Lin
426 *et al*. (submitted) examine NCP_{O2Ar} variability in the WAP from a community perspective
427 including top-down controls.
428
429 **3.3.1 Light Limitation and Freshwater Input**
430 We document a non-linear negative response of NCP_{O2Ar} to mixed layer depth whereby
431 NCP_{O2Ar} is consistently low when MLDs are greater than ~40 m and NCP_{O2Ar} is elevated and
432 more variable when MLDs are shallower than 40 m (Fig. 7a). Several studies in this region and

433 throughout the Southern Ocean have documented a consistent non-linear negative relationship
434 between the summer MLD and primary production [*Garibotti et al*., 2005; *Mitchell et al*., 1991;
435 *Mitchell and Holmhansen*, 1991; *Vernet et al*., 2008] and MLD and NCP_{O2Ar} [*Cassar et al*.,
436 2011; *Huang et al*., 2012; *Tortell et al*., 2015] with thresholds at 25-50 m. This suggests light
437 limitation, at least locally, at the WAP. We document independently this ~40 m threshold here
438 by comparing seasonal DIC drawdown ($\mathrm{nDIC}_w \cdot \rho_w - \mathrm{nDIC}_s \cdot \rho_s$) to mixed layer depth (Fig.
439 S5).

440 Freshwater input (meteoric and sea-ice meltwater) is a primary control on summertime
441 upper water column stability in the WAP [*Dierssen et al*., 2002; *Garibotti et al*., 2005; *Meredith*
442 *et al*., 2013; *Venables et al*., 2013; *Vernet et al*., 2008]. MLDs are generally shallower than ~25
443 m in the WAP when total meteoric and sea-ice meltwater content is greater than ~3.5% in the
444 surface. While it is clearly the case that freshwater inputs add buoyancy and lead to shallower
445 mixed layers, it should be noted that the nature of the relationship is also controlled by deep
446 mixing events diluting the surface freshwater fractions. Shallower mixed layers are also more
447 strongly stratified as indicated by the negative correlation between MLD and $\Delta\text{sigma-theta}_{Tmin\text{-}0}$
448 ($n=152$, $r^2=0.29$, $p<0.0001$) where $\Delta\text{sigma-theta}_{Tmin\text{-}0}$ is the potential density difference between
449 the winter water (defined by the water column temperature minimum) and the surface [*Saba et*
450 *al*., 2014].

451 Elevated meteoric water fraction and accompanying shallower, more stable mixed layers
452 are correlated with NCP_{O2Ar} in the WAP ($n=124$, $r^2=0.33$, $p<0.0001$, Fig. 7b). These correlations
453 are indicative of a bottom-up controlled, light-limited system that is critically sensitive to
454 freshwater inputs. Meteoric water, mixed layer depth, $\Delta\text{sigma-theta}_{Tmin\text{-}0}$ and NCP_{O2Ar} all exhibit
455 onshore-offshore gradients. The correlation could be an artifact of a corresponding spatial

456 gradient in an additional covarying property, such as Fe availability. The correlation between
457 NCP_{O2Ar} and meteoric water fraction is stronger than that between NCP_{O2Ar} and sea-ice
458 meltwater fraction, which may indicate the importance of glacial Fe input, as discussed below.
459
460 **3.3.2 Iron**
461 Surface dissolved and particulate Fe data available for 2012 indicate low concentrations
462 offshore and variable concentrations onshore (Fig. 8). Distinct declines in Fe with distance from
463 shore have been documented in the northern tip of the WAP [*Ardelan et al*., 2010], and more
464 recently in the Pal-LTER grid region (Sherrell *et al*., in prep). Because of biological uptake and
465 variable Fe speciation, dissolved Fe (dFe) concentration may however be a poor indicator of Fe
466 availability in the mixed layer [*Cassar et al*., 2011] and we cannot address the bioavailablility of
467 these Fe pools. Here we use dissolved manganese (dMn) concentration as a crude proxy for
468 recent Fe availability. Both dMn and dFe have similar physical supply mechanisms in the
469 Southern Ocean [*Measures et al*., 2013] but dMn is not scavenged biologically from the water
470 column as rapidly as dFe and thus can serve as a qualitative quasi-conservative indicator of
471 supply and subsequent horizontal dispersal by advection and diffusion in surface waters. We find
472 that dMn shows a strong correlation (Fig. 10b, n=21, r^2=0.76, p<0.0001) with Fv/Fm (Fig. 9), a
473 qualitative indicator of Fe stress [e.g. *Cassar et al*., 2011; *Hopkinson et al*., 2007; *Suggett et al*.,
474 2009; *Trimborn et al*., 2015] and a correlation with dFe (n=104, r^2=0.36, p<0.0001). Net
475 community production is positively correlated with dMn (Fig. 10a, n=72, r^2=0.26, p<0.0001).
476 Surface dMn concentration in 2012 displays a pronounced decline from the coastal region to
477 offshore (Fig. 8c). Dissolved Mn is also positively correlated with surface meteoric water
478 fraction (n=48, r^2=0.26, p<0.0005). While it is difficult to conclude whether this is an artifact of

479 coincident onshore-offshore gradients without causal relationship, it is consistent with our
480 current understanding of glacial runoff being an important delivery mechanism of trace metals to
481 the coastal region [*Hawkings et al*., 2014; *Huang et al*., 2012; *Sherrell et al*., 2015; *Vernet et al*.,
482 2008].

483 NCP_{O2Ar} is low offshore regardless of light availability as estimated from MLD or
484 stratification (Figs. 2, 7a,b). The consistently-observed low trace metal concentrations offshore
485 suggest Fe to be an important limiting factor for NCP_{O2Ar} in the area. These findings are
486 consistent with other studies that indicate offshore Fe limitation of primary production in the
487 pelagic Southern Ocean [e.g. *Cassar et al*., 2011; *de Baar et al*., 2005; *Martin et al*., 1990;
488 *Trimborn et al*., 2015]. However, these are the first published measurements to show that
489 dissolved Fe in (offshore) continental shelf waters can be as low as that in open Southern Ocean
490 surface waters (~0.1 nmol/kg), consistent with Fe limitation of diatoms and other phytoplankton
491 taxonomic groups [*Boyd et al*., 2000; *de Baar et al*., 1990; *Takeda*, 1998]. Further, the onshore-
492 offshore gradient in pFe is much stronger and more exponential in character than for dFe (Fig.
493 8). If some of this pFe is labile, it could be recycled on biologically relevant time scales and
494 contribute to the onshore high NCP_{O2Ar}. Fv/Fm also shows decreases from onshore to offshore
495 (Fig. 9). High Fv/Fm supports low Fe stress in the very near shore region especially in
496 Marguerite Bay and near Palmer Station (Fig. 9). While this discussion has focused on
497 meltwater-Fe relationships it is also important to note that sedimentary Fe sources may be
498 important in this region (Sherrell *et al*., in prep).

499 There is evidence of Fe limitation in the onshore regions (landward of grid station 100) as
500 seen by a significant positive correlation between NCP_{O2Ar} and Fv/Fm (Fig. 10c, n=10, r^2=0.31,
501 p=0.09 including only nighttime Fv/Fm data, Fig. 10d, n=66, r^2=0.11, p<0.01 when including all

Fv/Fm data). In these intermediate-status locations Fe and light may be co-limiting or limiting at different times in the growing season with bloom initiation in the spring dictated by stratification and light availability [*Tortell et al*., 2014; *Venables et al*., 2013] since Fe is generally replete in January in the coastal region (Sherrell *et al*., in prep), but with the ultimate magnitude of the bloom and the timing of the decline linked to Fe availability. Self-shading induced light limitation, grazing pressure [*Bernard et al*., 2012; *Garzio and Steinberg*, 2013] and community structure (Lin *et al*., submitted) are also likely key players in the bloom decline.

3.4 Interannual Variability

On average in the Pal-LTER region, ice retreat in 2014 was 11.5 days later than in 2012 and 18.8 days later than in 2013. This later ice retreat is manifested in the form of colder, fresher surface waters with shallower and more stable mixed layers and higher sea-ice meltwater fractions. Average measured NCP_{O2Ar} in 2014 was nearly double the rate in the previous two years. Production was particularly high in Marguerite Bay and near Palmer Station where it reached 413 mmol O_2 m^{-2} d^{-1}. As documented by *Tortell et al*. [2015], NCP_{O2Ar} was also this high in Marguerite Bay in January 2011, but it only reached ~140 mmol O_2 m^{-2} d^{-1} near Palmer Station at that time. Seasonal cycles of chlorophyll captured in time series sampling at two routinely sampled Pal-LTER sites near Palmer station show that the peak chlorophyll concentration occurred 15-30 days later in 2014 than it did in the 2012 and 2013 (Fig. 2). Peak chlorophyll concentration coincides with the ship sampling time in 2014 (though NCP might peak ~2 weeks later than chlorophyll [*Tortell et al*., 2014]). It is possible that NCP_{O2Ar} only appears highest in 2014 as a result of the bloom phenology and alignment with ship occupation. At RaTS, however, maximum chlorophyll concentration occurred at the same time or earlier than

525 the previous years and the concentration had diminished by the time of ship sampling in mid-
526 January. Therefore, timing does not appear to fully explain the observed interannual variability
527 in NCP_{O2Ar} in the southern onshore region. This is supported by satellite-derived NCP estimates
528 that show the mean January NCP in the onshore grid regions of the WAP in 2014 was
529 approximately double that observed in the previous two years (offshore magnitudes were
530 comparable year-to-year). While timing is certainly an important consideration when interpreting
531 our underway data, the $\tau_{O2}NCP_{O2Ar} : \Delta t\ NCP_{DIC}$ comparison (see section 3.2) also indicates that
532 timing cannot entirely explain the interannual variability at the WAP. Also, the nearshore
533 sampling locations at Palmer and Rothera Stations do not necessarily reflect bloom timing and
534 magnitude on the sampling grid.
535 Enhanced stability due to high meltwater fractions is a probable driver of elevated NCP.
536 Ice retreat occurs both by melting in situ, and from wind and ocean-driven sea-ice advection
537 [*Meredith et al*., 2013] (Meredith *et al*., in review, this issue) with important implications for
538 regional water column stability. In 2014, winds were such that ice retreat occurred by melting in
539 situ rather than net advection, resulting in more even sea-ice meltwater across the region
540 (Meredith *et al*., submitted, this issue) and lower mean SSS across the Pal-LTER grid. There
541 could have been a more widespread source of Fe from sea ice that was not yet depleted at the
542 time of our sampling. Sea ice may act as mobile seasonal reservoir of Fe that is incorporated into
543 the ice during formation in winter then released via meltwater in the spring and summer
544 [*Lannuzel et al*., 2008; *Sedwick and DiTullio*, 1997]. While dFe data are not available in all
545 years, in 2012 sea-ice meltwater content is correlated with surface dFe ($n=48$, $r^2=0.4$, $p<0.0001$),
546 supporting the notion that sea ice acts, at least to some extent, as an Fe delivery mechanism in
547 this region. Fv/Fm data indicate reduced iron stress offshore in 2014 compared to 2012 and

548 2013. Additionally meteoric water content is high along the coast in 2014 relative to the previous
549 years. Meteoric water is a combination of precipitation and glacial melt water, and both
550 freshwater inputs would have stabilization effects, however glacial melt water would potentially
551 represent a larger and more sustained Fe source.
552
553 **3.5 Spatial Variability**
554 **3.5.1 Ice Retreat**
555 As presented in our companion paper (Eveleth *et al*., in review b, this issue), biologically-
556 produced (or biotic) oxygen and pCO_2 display variability on the same spatial scales as salinity,
557 temperature and physical (abiotic) oxygen in the WAP (decorrelation length scale ~4.5 km)
558 bolstering the conclusion that NCP_{O2Ar} spatial variability is controlled by physical spatial
559 variability. Some spatial variability across the grid is likely a result of bloom stage at the time of
560 sampling. Ice retreat in our sampling region, defined as the date when sea-ice concentration
561 drops below 15% [*Stammerjohn et al*., 2008], occurred between 36 days before ship occupation
562 at a given location and 85 days after. While days of open water prior to ship sampling is not
563 significantly correlated to NCP_{O2Ar} magnitude at individual sampling points, perhaps because of
564 the relatively low resolution of the satellite ice data, we note large-scale spatial patterns across
565 the grid that are consistent with the well-known ice retreat-primary production progression (Fig.
566 11). Retreat occurred predominantly from offshore to onshore in 2012 and the NCP_{O2Ar} gradient
567 in this direction is prominent. In 2013, ice retreated from north to south and we observe a strong
568 N-S gradient in NCP_{O2Ar} with higher values in the southern grid region related to later ice retreat.
569 In 2014, ice retreat was late across most of the region, and there was high NCP_{O2Ar} throughout
570 the coastal region. We also note isolated very fresh regions (salinity ~30-32) in 2012 and 2014

571 that are likely recent freshwater melt lenses that have not yet had time to develop blooms and
572 NCP_{O2Ar} is near zero (Fig. S6). As discussed above, while timing is an important consideration, it
573 likely does not fully describe the documented spatial variability. Rather than phenology, the
574 large-scale spatial patterns in NCP_{O2Ar} could be a function of sea ice-driven water column
575 stability and/or Fe injection at the site of sea-ice melt [*Boyd and Ellwood*, 2010; *Lannuzel et al*.,
576 2008] (See maps of all data Fig. S7).
577
578 **3.5.2 Canyons**
579 Much attention in the current WAP literature has been paid to productivity at canyon
580 hotspots [*Ducklow et al*., 2013; *Kavanaugh et al*., 2015; *Oliver et al*., 2013; *Prezelin et al*., 2000;
581 *Schofield et al*., 2013]. Near the 600, 400 and 200 gridlines major penguin breeding colonies on
582 Anvers Island, Renaud Island, and Avian Island have been shown to be co-located with high
583 chlorophyll and krill concentrations and deep cross-shelf cutting canyons [*Kavanaugh et al*.,
584 2015; *Schofield et al*., 2013; *Smith et al*., 1998]. By visual inspection, NCP_{O2Ar} rates near the
585 canyons also appear elevated relative to the rest of the coastal region. Though this is difficult to
586 show statistically here, it can additionally be seen in the satellite-derived annual NCP_{O2Ar}
587 climatology (Li *et al*., in review). Canyons are believed to act as conduits for the UCDW that
588 carries heat and macro- and micro-nutrients to the near shore region [e.g. *Kavanaugh et al*.,
589 2015; *Martinson et al*., 2008; *Prezelin et al*., 2000; *Schofield et al*., 2013]. The relatively high
590 SST over the canyons is linked to shallower mixed layer depths and localized earlier ice retreat
591 (as seen in 2014, Fig. 11) and longer growing seasons [*Kavanaugh et al*., 2015]. UCDW might
592 pick up additional sedimentary-sourced Fe as it travels across the shelf [*Marsay et al*., 2014].
593 When these waters obduct to the surface layer, as suggested by the elevated SST [*Kavanaugh et*

594 *al*., 2015] and observed upwelling from glider transects near Palmer Deep [*Schofield et al*.,
595 2013], they would likely deliver enhanced concentrations of micronutrients including Fe.
596 Although not conclusive, surface pFe and dMn are elevated in Marguerite Bay (onshore 200
597 line) and near Palmer Station (onshore 600 line) relative to other coastal areas in 2012. Ongoing
598 horizontal and vertical trace metal surveys being conducted as part of the Pal-LTER program
599 will elucidate Fe supply mechanisms in the WAP including the possible role of canyons as
600 conduits for limiting nutrients.
601
602 **4. Conclusions**
603 In the austral summers of 2012-2014, the Pal-LTER grid region of the WAP was a net
604 carbon sink with particularly high NCP in the coastal region and at hotspots associated with
605 submarine canyons. Sea ice appears to be an important driver of NCP_{O2Ar}, likely by stabilizing
606 the summer mixed layer via meltwater input and limiting deep wind-driven winter mixing, and
607 serving as transient Fe storage with seasonal delivery. Meteoric water, both glacial meltwater
608 and precipitation, also acts as a stabilizing force in the region, particularly where input is high
609 along the coast. Glacial meltwater may also be an important source of Fe to the region. Fe stress
610 is widespread in the offshore region, farthest from this meltwater Fe source. In the near coastal
611 zone, Fe stress is low thus high and variable NCP_{O2Ar} in coastal waters is more related to mixed
612 layer stratification as it controls both light availability and timing. Further from the coast but still
613 on the shelf (~gridlines 20 to 100) we see local indications of both Fe and light limitation.
614 Controls on summer NCP_{O2Ar} are closely tied to sea ice and glacial melt, both of which
615 are changing in the rapidly warming climate [*Meredith et al*., 2013; *Stammerjohn et al*., 2008;
616 *Vaughan*, 2006]. If sea ice continues its current trend and melts earlier in the spring, surface

water would be exposed to stronger winds and deeper mixing, assuming the winds were strong enough to overcome otherwise warmer more defined surface layers due to increased solar heating. This may distribute the meltwater over a greater depth range, and also promote advection away from input locations [*Venables et al*., 2013] (Meredith *et al*., in review, this issue). Physical wind mixing and reduction in surface meltwater would both weaken summer stratification, perhaps increasing light limitation but potentially increasing upward mixing of Fe-rich subsurface water. Deeper mixing and weaker stratification due to early sea-ice retreat may be countered by enhanced glacial melt water input along the coast [*Vaughan*, 2006]. This melt water may also enhance Fe input and relieve micronutrient limitation onshore. With the multitude of processes involved, it remains challenging to predict how NCP might respond to these potential changes in the WAP and other areas of current and expected future warming in both polar regions. However, given the observed connections with meltwater, stratification and Fe we expect NCP to be sensitive to the changing climate and ongoing sustained observation programs, such as Pal-LTER and RaTS, and high-spatial resolution measurements are critical to developing the needed understanding.

Acknowledgements

We would like to thank two anonymous reviewers for their insightful comments. Thank you to the logistics support, officers, scientists and crew of the ARSV LMG for help with data collection, and Sharon Stammerjohn, Oscar Schofield, Claudine Hauri, Adam Ulfsbo and Rich Iannuzzi for valuable contributions of data and insight. RaTS is a component of the British Antarctic Survey's Polar Oceans program, funded by the Natural Environment Research Council. We thank all those concerned with the collection of RaTS samples and data including the

640 Rothera Marine Assistants. This material is based upon work supported by the National Science
641 Foundation Graduate Research Fellowship Program under Grant No. 1106401. Work was
642 supported by NSF OPP-1043339 to N.C., NSF awards PLR-1344502 and 1440435 (Palmer
643 LTER Project) to H.W.D at Columbia University. The research was additionally supported by
644 the LTER Program of the US National Science Foundation (ANT-0823101) and NSF ANT-
645 0838995 to R.M.S.

646

647

648 **References**

649 Allison, D. B., D. Stramski, and B. G. Mitchell (2010), Seasonal and interannual variability of
650 particulate organic carbon within the Southern Ocean from satellite ocean color observations, *J*
651 *Geophys Res-Oceans*, *115*, doi:10.1029/2009jc005347.

652 Anadon, R., F. Alvarez-Marques, E. Fernandez, M. Varela, M. Zapata, J. M. Gasol, and D.
653 Vaque (2002), Vertical biogenic particle flux during Austral summer in the Antarctic Peninsula
654 area, *Deep-Sea Res Pt Ii*, *49*(4-5), 883-901, doi:10.1016/S0967-0645(01)00129-1.

655 Ardelan, M. V., O. Holm-Hansen, C. D. Hewes, C. S. Reiss, N. S. Silva, H. Dulaiova, E.
656 Steinnes, and E. Sakshaug (2010), Natural iron enrichment around the Antarctic Peninsula in the
657 Southern Ocean, *Biogeosciences*, *7*(1), 11-25.

658 Bender, M. L., S. Kinter, N. Cassar, and R. Wanninkhof (2011), Evaluating gas transfer velocity
659 parameterizations using upper ocean radon distributions, *J Geophys Res-Oceans*, *116*,
660 doi:10.1029/2009jc005805.

661 Bernard, K. S., D. K. Steinberg, and O. M. E. Schofield (2012), Summertime grazing impact of
662 the dominant macrozooplankton off the Western Antarctic Peninsula, *Deep-Sea Res Pt I*, *62*,
663 111-122, doi:10.1016/j.dsr.2011.12.015.

664 Boyd, P. W., and M. J. Ellwood (2010), The biogeochemical cycle of iron in the ocean, *Nat*
665 *Geosci*, *3*(10), 675-682, doi:10.1038/Ngeo964.

666 Boyd, P. W., et al. (2000), A mesoscale phytoplankton bloom in the polar Southern Ocean
667 stimulated by iron fertilization, *Nature*, *407*(6805), 695-702, doi:10.1038/35037500.

668 Carlson, C. A., S. J. Giovannoni, D. A. Hansell, S. J. Goldberg, R. Parsons, M. P. Otero, K.
669 Vergin, and B. R. Wheeler (2002), Effect of nutrient amendments on bacterioplankton
670 production, community structure, and DOC utilization in the northwestern Sargasso Sea, *Aquat*
671 *Microb Ecol*, *30*(1), 19-36, doi:10.3354/ame030019.

672 Carrillo, C. J., R. C. Smith, and D. M. Karl (2004), Processes regulating oxygen and carbon
673 dioxide in surface waters west of the Antarctic Peninsula, *Mar*. *Chem*., *84*(3-4), 161-179,
674 doi:10.1016/j.marchem.2003.07.004.

675 Cassar, N., B. A. Barnett, M. L. Bender, J. Kaiser, R. C. Hamme, and B. Tilbrook (2009),
676 Continuous High-Frequency Dissolved O-2/Ar Measurements by Equilibrator Inlet Mass
677 Spectrometry, *Anal Chem*, *81*(5), 1855-1864, doi:10.1021/Ac802300u.

678 Cassar, N., M. L. Bender, B. A. Barnett, S. Fan, W. J. Moxim, H. Levy, and B. Tilbrook (2007),
679 The Southern Ocean biological response to Aeolian iron deposition, *Science*, *317*(5841), 1067-
680 1070, doi:10.1126/science.1144602.

681 Cassar, N., P. J. DiFiore, B. A. Barnett, M. L. Bender, A. R. Bowie, B. Tilbrook, K. Petrou, K. J.
682 Westwood, S. W. Wright, and D. Lefevre (2011), The influence of iron and light on net
683 community production in the Subantarctic and Polar Frontal Zones, *Biogeosciences*, *8*(2), 227-
684 237, doi:10.5194/Bg-8-227-2011.

685 Cassar, N., C. D. Nevison, and M. Manizza (2014), Correcting oceanic O-2/Ar-net community
686 production estimates for vertical mixing using N2O observations, *Geophys Res Lett*, *41*(24),
687 8961-8970, doi:10.1002/2014gl062040.

688 Clarke, A., M. P. Meredith, M. I. Wallace, M. A. Brandon, and D. N. Thomas (2008), Seasonal
689 and interannual variability in temperature, chlorophyll and macronutrients in northern
690 Marguerite Bay, Antarctica, *Deep-Sea Res Pt Ii*, *55*(18-19), 1988-2006,
691 doi:10.1016/j.dsr2.2008.04.035.

692 de Baar, H. J. W., et al. (2005), Synthesis of iron fertilization experiments: From the iron age in
693 the age of enlightenment, *J Geophys Res-Oceans*, *110*(C9), doi:10.1029/2004jc002601.

694 de Baar, H. J. W., A. G. J. Buma, R. F. Nolting, G. C. Cadee, G. Jacques, and P. J. Treguer
695 (1990), On Iron Limitation of the Southern-Ocean - Experimental-Observations in the Weddell
696 and Scotia Seas, *Mar Ecol Prog Ser*, *65*(2), 105-122, doi:10.3354/meps065105.

697 Dickson, A. G. (1990), Thermodynamics of the Dissociation of Boric-Acid in Synthetic
698 Seawater from 273.15-K to 318.15-K, *Deep-Sea Res*, *37*(5), 755-766, doi:10.1016/0198-
699 0149(90)90004-F.

700 Dierssen, H. M., R. C. Smith, and M. Vernet (2002), Glacial meltwater dynamics in coastal
701 waters west of the Antarctic peninsula, *P Natl Acad Sci USA*, *99*(4), 1790-1795,
702 doi:10.1073/Pnas.032206999.

703 Ducklow, H. W., K. Baker, D. G. Martinson, L. B. Quetin, R. M. Ross, R. C. Smith, S. E.
704 Stammerjohn, M. Vernet, and W. Fraser (2007), Marine pelagic ecosystems: The West Antarctic
705 Peninsula, *Philos T R Soc B*, *362*(1477), 67-94, doi:10.1098/Rstb.2006.1955.

706 Ducklow, H. W., et al. (2013), West Antarctic Peninsula: An Ice-Dependent Coastal Marine
707 Ecosystem in Transition, *Oceanography*, *26*(3), 190-203.

708 Ducklow, H. W., O. Schofield, M. Vernet, S. Stammerjohn, and M. Erickson (2012), Multiscale
709 control of bacterial production by phytoplankton dynamics and sea ice along the western
710 Antarctic Peninsula: A regional and decadal investigation, *Journal of Marine Systems*, *98-99*, 26-
711 39, doi:10.1016/j.jmarsys.2012.03.003.

712 Epstein, S., and T. Mayeda (1953), Variation of O-18 Content of Waters from Natural Sources,
713 *Geochim Cosmochim Ac*, *4*(5), 213-224, doi:10.1016/0016-7037(53)90051-9.

714 Espinasse, B., M. Zhou, Y. W. Zhu, E. L. Hazen, A. S. Friedlaender, D. P. Nowacek, D. Z. Chu,
715 and F. Carlotti (2012), Austral fall-winter transition of mesozooplankton assemblages and krill
716 aggregations in an embayment west of the Antarctic Peninsula, *Mar Ecol Prog Ser*, *452*, 63-80,
717 doi:10.3354/Meps09626.

718 Eveleth, R., M. L. Timmermans, and N. Cassar (2014), Physical and biological controls on
719 oxygen saturation variability in the upper Arctic Ocean, *J Geophys Res-Oceans*, *119*(11), 7420-
720 7432, doi:10.1002/2014jc009816.

721 Garcia, H. E., and L. I. Gordon (1992), Oxygen Solubility in Seawater - Better Fitting Equations,
722 *Limnol Oceanogr*, *37*(6), 1307-1312.

723 Garibotti, I. A., M. Vernet, R. C. Smith, and M. E. Ferrario (2005), Interannual variability in the
724 distribution of the phytoplankton standing stock across the seasonal sea-ice zone west of the
725 Antarctic Peninsula, *J Plankton Res*, *27*(8), 825-843, doi:10.1093/Plankt/Fbi056.

726 Garzio, L. M., and D. K. Steinberg (2013), Microzooplankton community composition along the
727 Western Antarctic Peninsula, *Deep-Sea Res Pt I*, *77*, 36-49, doi:10.1016/j.dsr.2013.03.001.

728 Giesbrecht, K. E., R. C. Hamme, and S. R. Emerson (2012), Biological productivity along Line P
729 in the subarctic northeast Pacific: In situ versus incubation-based methods, *Global Biogeochem*
730 *Cy*, *26*, doi:10.1029/2012gb004349.

731 Gorbunov, M. Y., Z. S. Kolber, and P. G. Falkowski (1999), Measuring photosynthetic
732 parameters in individual algal cells by Fast Repetition Rate fluorometry, *Photosynth Res*, *62*(2-
733 3), 141-153, doi:10.1023/A:1006360005033.

734 Hamme, R. C., et al. (2012), Dissolved O-2/Ar and other methods reveal rapid changes in
735 productivity during a Lagrangian experiment in the Southern Ocean, *J Geophys Res-Oceans*,
736 *117*, doi:10.1029/2011jc007046.

737 Hamme, R. C., and S. R. Emerson (2004), The solubility of neon, nitrogen and argon in distilled
738 water and seawater, *Deep-Sea Res Pt I*, *51*(11), 1517-1528, doi:10.1016/J.Dsr.2004.06.009.

739 Hansell, D. A., and C. A. Carlson (1998), Net community production of dissolved organic
740 carbon, *Global Biogeochem Cy*, *12*(3), 443-453, doi:10.1029/98gb01928.

741 Hauri, C., S. C. Doney, T. Takahashi, M. Erickson, G. Jiang, and H. W. Ducklow (2015), Two
742 decades of inorganic carbon dynamics along the Western Antarctic Peninsula, *Biogeosciences*
743 *Discuss*., *12*(9), 6929-6969, doi:10.5194/bgd-12-6929-2015.

744 Hawkings, J. R., J. L. Wadham, M. Tranter, R. Raiswell, L. G. Benning, P. J. Statham, A.
745 Tedstone, P. Nienow, K. Lee, and J. Telling (2014), Ice sheets as a significant source of highly
746 reactive nanoparticulate iron to the oceans, *Nat Commun*, *5*, doi:10.1038/ncomms4929.

747 Hopkinson, B. M., G. Mitchell, R. A. Reynolds, H. Wang, K. E. Selph, C. I. Measures, C. D.
748 Hewes, O. Holm-Hansen, and K. A. Barbeau (2007), Iron limitation across chlorophyll gradients
749 in the southern Drake Passage: Phytoplankton responses to iron addition and photosynthetic
750 indicators of iron stress, *Limnol Oceanogr*, *52*(6), 2540-2554, doi:10.4319/Lo.2007.52.6.2540.

751 Huang, K., H. Ducklow, M. Vernet, N. Cassar, and M. L. Bender (2012), Export production and
752 its regulating factors in the West Antarctica Peninsula region of the Southern Ocean, *Global*
753 *Biogeochem Cy*, *26*, doi:10.1029/2010gb004028.

754 Ishii, M., H. Y. Inoue, and H. Matsueda (2002), Net community production in the marginal ice
755 zone and its importance for the variability of the oceanic pCO(2) in the Southern Ocean south of
756 Australia, *Deep-Sea Res Pt Ii*, *49*(9-10), 1691-1706, doi:10.1016/S0967-0645(02)00007-3.

757 Jonsson, B. F., S. C. Doney, J. Dunne, and M. Bender (2013), Evaluation of the Southern Ocean
758 O-2/Ar-based NCP estimates in a model framework, *J Geophys Res-Biogeo*, *118*(2), 385-399,
759 doi:10.1002/Jgrg.20032.

760 Juranek, L. W., R. C. Hamme, J. Kaiser, R. Wanninkhof, and P. D. Quay (2010), Evidence of O-
761 2 consumption in underway seawater lines: Implications for air-sea O-2 and CO2 fluxes,
762 *Geophys Res Lett*, *37*, doi:10.1029/2009gl040423.

763 Karl, D. M. (1991), Racer - Research on Antarctic Coastal Ecosystem Rates - Preface, *Deep-Sea*
764 *Res*, *38*(8-9), R5-R7, doi:10.1016/0198-0149(91)90089-X.

765 Kavanaugh, M. T., F. N. Abdala, H. Ducklow, D. Glover, W. Fraser, D. Martinson, S.
766 Stammerjohn, O. Schofield, and S. C. Doney (2015), Effect of continental shelf canyons on
767 phytoplankton biomass and community composition along the western Antarctic Peninsula, *Mar*
768 *Ecol Prog Ser*, *524*, 11-26, doi:10.3354/Meps11189.

769 Lagerström, M. E., M. P. Field, M. Seguret, L. Fischer, S. Hann, and R. M. Sherrell (2013),
770 Automated on-line flow-injection ICP-MS determination of trace metals (Mn, Fe, Co, Ni, Cu and
771 Zn) in open ocean seawater: Application to the GEOTRACES program, *Mar*. *Chem*., *155*, 71-80,
772 doi:10.1016/j.marchem.2013.06.001.

773 Lannuzel, D., V. Schoemann, J. de Jong, L. Chou, B. Delille, S. Becquevort, and J. L. Tison
774 (2008), Iron study during a time series in the western Weddell pack ice, *Mar*. *Chem*., *108*(1-2),
775 85-95, doi:10.1016/J.Marchem.2007.10.006.

776 Laws, E. A. (1991), Photosynthetic Quotients, New Production and Net Community Production
777 in the Open Ocean, *Deep-Sea Res*, *38*(1), 143-167, doi:10.1016/0198-0149(91)90059-O.

778 Lueker, T. J., A. G. Dickson, and C. D. Keeling (2000), Ocean pCO(2) calculated from dissolved
779 inorganic carbon, alkalinity, and equations for K-1 and K-2: validation based on laboratory
780 measurements of CO2 in gas and seawater at equilibrium, *Mar*. *Chem*., *70*(1-3), 105-119,
781 doi:10.1016/S0304-4203(00)00022-0.

782 Marsay, C. M., P. N. Sedwick, M. S. Dinniman, P. M. Barrett, S. L. Mack, and D. J.
783 McGillicuddy (2014), Estimating the benthic efflux of dissolved iron on the Ross Sea continental
784 shelf, *Geophys Res Lett*, *41*(21), 7576-7583, doi:10.1002/2014gl061684.

785 Martin, J. H., R. M. Gordon, and S. E. Fitzwater (1990), Iron in Antarctic Waters, *Nature*,
786 *345*(6271), 156-158, doi:10.1038/345156a0.

787 Martinson, D. G., S. E. Stammerjohn, R. A. Iannuzzi, R. C. Smith, and M. Vernet (2008),
788 Western Antarctic Peninsula physical oceanography and spatio-temporal variability, *Deep-Sea*
789 *Res Pt Ii*, *55*(18-19), 1964-1987, doi:10.1016/J.Dsr2.2008.04.038.

790 Measures, C. I., M. T. Brown, K. E. Selph, A. Apprill, M. Zhou, M. Hatta, and W. T. Hiscock
791 (2013), The influence of shelf processes in delivering dissolved iron to the HNLC waters of the
792 Drake Passage, Antarctica, *Deep-Sea Res Pt Ii*, *90*, 77-88, doi:10.1016/J.Dsr2.2012.11.004.

793 Meredith, M. P., H. J. Venables, A. Clarke, H. W. Ducklow, M. Erickson, M. J. Leng, J. T. M.
794 Lenaerts, and M. R. van den Broeke (2013), The Freshwater System West of the Antarctic
795 Peninsula: Spatial and Temporal Changes, *J Climate*, *26*(5), 1669-1684, doi:10.1175/Jcli-D-12-
796 00246.1.

797 Mitchell, B. G., E. A. Brody, O. Holmhansen, C. Mcclain, and J. Bishop (1991), Light
798 Limitation of Phytoplankton Biomass and Macronutrient Utilization in the Southern-Ocean,
799 *Limnol Oceanogr*, *36*(8), 1662-1677.

800 Mitchell, B. G., and O. Holmhansen (1991), Observations and Modeling of the Antarctic
801 Phytoplankton Crop in Relation to Mixing Depth, *Deep-Sea Res*, *38*(8-9), 981-1007,
802 doi:10.1016/0198-0149(91)90093-U.

803 Monterey, G. I., and S. Levitus (1997), Seasonal variability of mixed layer depth for the world
804 ocean, in *NOA Atlas NESDIS 14*, edited, p. 96, U.S. Government Printing Office, Washington,
805 D.C.

806 Montes-Hugo, M., S. C. Doney, H. W. Ducklow, W. Fraser, D. Martinson, S. E. Stammerjohn,
807 and O. Schofield (2009), Recent Changes in Phytoplankton Communities Associated with Rapid
808 Regional Climate Change Along the Western Antarctic Peninsula, *Science*, *323*(5920), 1470-
809 1473, doi:10.1126/Science.1164533.

810 Munro, D. R., N. S. Lovenduski, B. B. Stephens, T. Newberger, K. R. Arrigo, T. Takahashi, P.
811 D. Quay, J. Sprintall, N. Freeman, and C. Sweeney (2015), Estimates of net community
812 production in the southern ocean determined from time series observations (2002–2011) of
813 nutrients, dissolved inorganic carbon, and surface ocean pCO2 in drake passage, *Deep Sea*
814 *Research Part II: Topical Studies in Oceanography*(0), doi:10.1016/j.dsr2.2014.12.014.

Nowacek, D. P., A. S. Friedlaender, P. N. Halpin, E. L. Hazen, D. W. Johnston, A. J. Read, B. Espinasse, M. Zhou, and Y. W. Zhu (2011), Super-Aggregations of Krill and Humpback Whales in Wilhelmina Bay, Antarctic Peninsula, *Plos One*, *6*(4), doi:10.1371/journal.pone.0019173.

Oliver, M. J., A. Irwin, M. A. Moline, W. Fraser, D. Patterson, O. Schofield, and J. Kohut (2013), Adelie Penguin Foraging Location Predicted by Tidal Regime Switching, *Plos One*, *8*(1), doi:ARTN e55163
10.1371/journal.pone.0055163.

Planquette, H., and R. M. Sherrell (2012), Sampling for particulate trace element determination using water sampling bottles: methodology and comparison to in situ pumps, *Limnol Oceanogr-Meth*, *10*, 367-388, doi:10.4319/lom.2012.10.367.

Prezelin, B. B., E. E. Hofmann, C. Mengelt, and J. M. Klinck (2000), The linkage between Upper Circumpolar Deep Water (UCDW) and phytoplankton assemblages on the west Antarctic Peninsula continental shelf, *J Mar Res*, *58*(2), 165-202, doi:10.1357/002224000321511133.

Reuer, M. K., B. A. Barnett, M. L. Bender, P. G. Falkowski, and M. B. Hendricks (2007), New estimates of Southern Ocean biological production rates from O-2/Ar ratios and the triple isotope composition of O-2, *Deep-Sea Res Pt I*, *54*(6), 951-974, doi:10.1016/J.Dsr.2007.02.007.

Saba, G. K., et al. (2014), Winter and spring controls on the summer food web of the coastal West Antarctic Peninsula, *Nat Commun*, *5*, doi:10.1038/Ncomms5318.

Schofield, O., et al. (2013), Penguin Biogeography Along the West Antarctic Peninsula Testing the Canyon Hypothesis with Palmer LTER Observations, *Oceanography*, *26*(3), 204-206.

Sedwick, P. N., and G. R. DiTullio (1997), Regulation of algal blooms in Antarctic shelf waters by the release of iron from melting sea ice, *Geophys Res Lett*, *24*(20), 2515-2518, doi:10.1029/97gl02596.

Sherrell, R. M., M. Lagerstrom, K. O. Forsch, S. Stammerjohn, and P. L. Yager (2015), Dynamics of dissolved iron and other bioactive trace metlas (Mn, Ni, Cu, Zn) in the Amundsen Sea Polynya, Antarctica, *Elem Sci Anth*, *3*(000071), doi:10.12952/journal.elementa.000071.

Smith, R. C., K. S. Baker, and P. Dustan (1981), Fluorometric techniques for the measurement of oceanic chlorophyll in the support of remote sensing*Rep*., Scripps Inst. of Oceanogr., San Diego, Calif.

844 Smith, R. C., K. S. Baker, and M. Vernet (1998), Seasonal and interannual variability of
845 phytoplankton biomass west of the Antarctic Peninsula, *Journal of Marine Systems*, *17*(1-4),
846 229-243, doi:10.1016/S0924-7963(98)00040-2.

847 Stammerjohn, S. E., D. G. Martinson, R. C. Smith, and R. A. Iannuzzi (2008), Sea ice in the
848 western Antarctic Peninsula region: Spatio-temporal variability from ecological and climate
849 change perspectives, *Deep-Sea Res Pt Ii*, *55*(18-19), 2041-2058,
850 doi:10.1016/J.Dsr2.2008.04.026.

851 Steinberg, D. K., K. E. Ruck, M. R. Gleiber, L. M. Garzio, J. S. Cope, K. S. Bernard, S. E.
852 Stammerjohn, O. M. E. Schofield, L. B. Quetin, and R. M. Ross (2015), Long-term (1993-2013)
853 changes in macrozooplankton off the Western Antarctic Peninsula, *Deep-Sea Res Pt I*, *101*, 54-
854 70, doi:10.1016/j.dsr.2015.02.009.

855 Suggett, D. J., C. M. Moore, A. E. Hickman, and R. J. Geider (2009), Interpretation of fast
856 repetition rate (FRR) fluorescence: signatures of phytoplankton community structure versus
857 physiological state, *Mar Ecol Prog Ser*, *376*, 1-19, doi:10.3354/meps07830.

858 Sweeney, C., D. A. Hansell, C. A. Carlson, L. A. Codispoti, L. I. Gordon, J. Marra, F. J. Millero,
859 W. O. Smith, and T. Takahashi (2000), Biogeochemical regimes, net community production and
860 carbon export in the Ross Sea, Antarctica, *Deep-Sea Res Pt Ii*, *47*(15-16), 3369-3394,
861 doi:10.1016/S0967-0645(00)00072-2.

862 Takeda, S. (1998), Influence of iron availability on nutrient consumption ratio of diatoms in
863 oceanic waters, *Nature*, *393*(6687), 774-777, doi:10.1038/31674.

864 Top, Z., S. Martin, and P. Becker (1988), A Laboratory Study of Dissolved Noble-Gas Anomaly
865 Due to Ice Formation, *Geophys Res Lett*, *15*(8), 796-799, doi:10.1029/Gl015i008p00796.

866 Tortell, P. D., E. C. Asher, H. W. Ducklow, J. A. L. Goldman, J. W. H. Dacey, J. J. Grzymski, J.
867 N. Young, S. A. Kranz, K. S. Bernard, and F. M. M. Morel (2014), Metabolic balance of coastal
868 Antarctic waters revealed by autonomous pCO2 and ΔO2/Ar measurements, *Geophys Res Lett*,
869 *41*(19), 2014GL061266, doi:10.1002/2014GL061266.

870 Tortell, P. D., H. C. Bittig, A. Körtzinger, E. M. Jones, and M. Hoppema (2015), Biological and
871 physical controls on N2, O2 and CO2 distributions in contrasting Southern Ocean surface waters,
872 *Global Biogeochem Cy*, doi:10.1002/2014GB004975.

873 Trimborn, S., C. J. M. Hoppe, B. B. Taylor, A. Bracher, and C. Hassler (2015), Physiological
874 characteristics of open ocean and coastal phytoplankton communities of Western Antarctic

875 Peninsula and Drake Passage waters, *Deep-Sea Res Pt I*, *98*, 115-124,
876 doi:10.1016/J.Dsr.2014.12.010.

877 van Heuven, S., D. Pierrot, J. W. B. Rae, E. Lewis, and D. W. R. Wallace (2011), MATLAB
878 Program Developed for CO2 System Calculations., ORNL/CDIAC-105b, edited, Carbon
879 Dioxide Information Analysis Center, Oak Ridge National Laboratory, U.S.
880 Department of Energy, Oak Ridge, Tennessee.,
881 doi:10.3334/CDIAC/otg.CO2SYS_MATLAB_v1.1.

882 Vaughan, D. G. (2006), Recent trends in melting conditions on the Antarctic Peninsula and their
883 implications for ice-sheet mass balance and sea level, *Arct Antarct Alp Res*, *38*(1), 147-152,
884 doi:10.1657/1523-0430(2006)038[0147:Rtimco]2.0.Co;2.

885 Venables, H. J., A. Clarke, and M. P. Meredith (2013), Wintertime controls on summer
886 stratification and productivity at the western Antarctic Peninsula, *Limnol Oceanogr*, *58*(3), 1035-
887 1047, doi:10.4319/Lo.2013.58.3.1035.

888 Vernet, M., D. Martinson, R. Iannuzzi, S. Stammerjohn, W. Kozlowski, K. Sines, R. Smith, and
889 I. Garibotti (2008), Primary production within the sea-ice zone west of the Antarctic Peninsula:
890 I-Sea ice, summer mixed layer, and irradiance, *Deep-Sea Res Pt Ii*, *55*(18-19), 2068-2085,
891 doi:10.1016/J.Dsr2.2008.05.021.

892 Wanninkhof, R. (1992), Relationship between Wind-Speed and Gas-Exchange over the Ocean, *J*
893 *Geophys Res-Oceans*, *97*(C5), 7373-7382, doi:10.1029/92jc00188.
894

895

896

897

898 **Figure Captions**

899 Fig. 1. Bathymetry of the Western Antarctic Peninsula on the Pal-LTER grid with key regions
900 and currents indicated. Transparent white lines indicate sampling grid lines during the Pal LTER
901 annual cruise. Station B, Station E and RaTS are marked by the purple, red and yellow stars
902 respectively. Deep currents shown in gray and surface currents in black (dotted if less certain) as
903 modified from Meredith *et al*. [2013].
904
905 Fig. 2. Near surface (5 m) Chl a concentration time series in 2012 (top), 2013 (middle) and 2014
906 (bottom) at Palmer Station B (blue line, purple star Fig 1), Station E (red-orange line, red star Fig

1) and RaTS (yellow line, yellow star Fig 1). Shaded box indicates time window of Pal-LTER annual cruise sampling.

Fig. 3. NCP_{O2Ar} in austral summer 2012 (left), 2013 (center) and 2014 (right) on the Pal-LTER grid. Thin gray line is the 500 m isobath. Black, blue and red boxes mark the designated offshore, northern onshore and southern onshore sub-regions.

Fig. 4. Mean NCP_{O2Ar} (± 1σ) in three regions of the Pal-LTER grid in 2012 (black), 2013 (gray) and 2014 (white). Regions defined as in Figure 3.

Fig. 5. Biological oxygen inventory vs. seasonal DIC drawdown in the Pal-LTER grid region in 2012 (green), 2013 (blue) and 2014 (cyan). Solid line is the 1:1 line and dotted line is the least-squared regression line for all three years with slope 0.37 and r^2 0.83.

Fig. 6. NCP_{O2Ar} vs. surface (~5 m) Chl a concentration in the Pal-LTER grid region with least squares regression (r^2=0.54). Symbols denote grid region as defined in Figure 3.

Fig. 7. a) NCP_{O2Ar} vs. MLD colored by grid station (low values coastal, high values offshore) in all years with regional symbol shape as in c. b.) NCP_{O2Ar} vs. near surface meteoric water fraction with color indicating upper water column stratification and symbol size representing relative MLD with larger symbols for deeper MLDs.

Fig. 8. Surface (5 m) dissolved Fe (left), particulate Fe (middle) and dissolved Mn (right) concentrations in 2012. Maximum pFe concentration was 21.05 nmol kg^{-1}.

Fig. 9. All surface F_v/F_m in 2012 (left), 2013 (middle) and 2014 (right).

Fig. 10. a.) NCP_{O2Ar} vs. dMn concentration in 2012, as an indicator of Fe availability. b.) Correlation of Fv/Fm and dMn (all day) in 2012. c.) NCP_{O2Ar} vs. nighttime Fv/Fm in all years. d.) NCP_{O2Ar} vs. all Fv/Fm data in all years. Symbols denote sub-regions defined in Figure 3. Model II linear least squares bisector regressions shown.

Fig. 11. Ice retreat for 2012 (left), 2013 (middle) and 2014 (right) in year day defined as the number of days since the previous year's sea ice minimum (~Feb 15). For example, the left plot shows the number of days since Feb 15, 2011 and thus the relevant ice retreat for the 2012 sampling cruise. NCP_{O2Ar} (mmol O_2 m^{-2} d^{-1}) overlaid in gray scale.

Figure 1

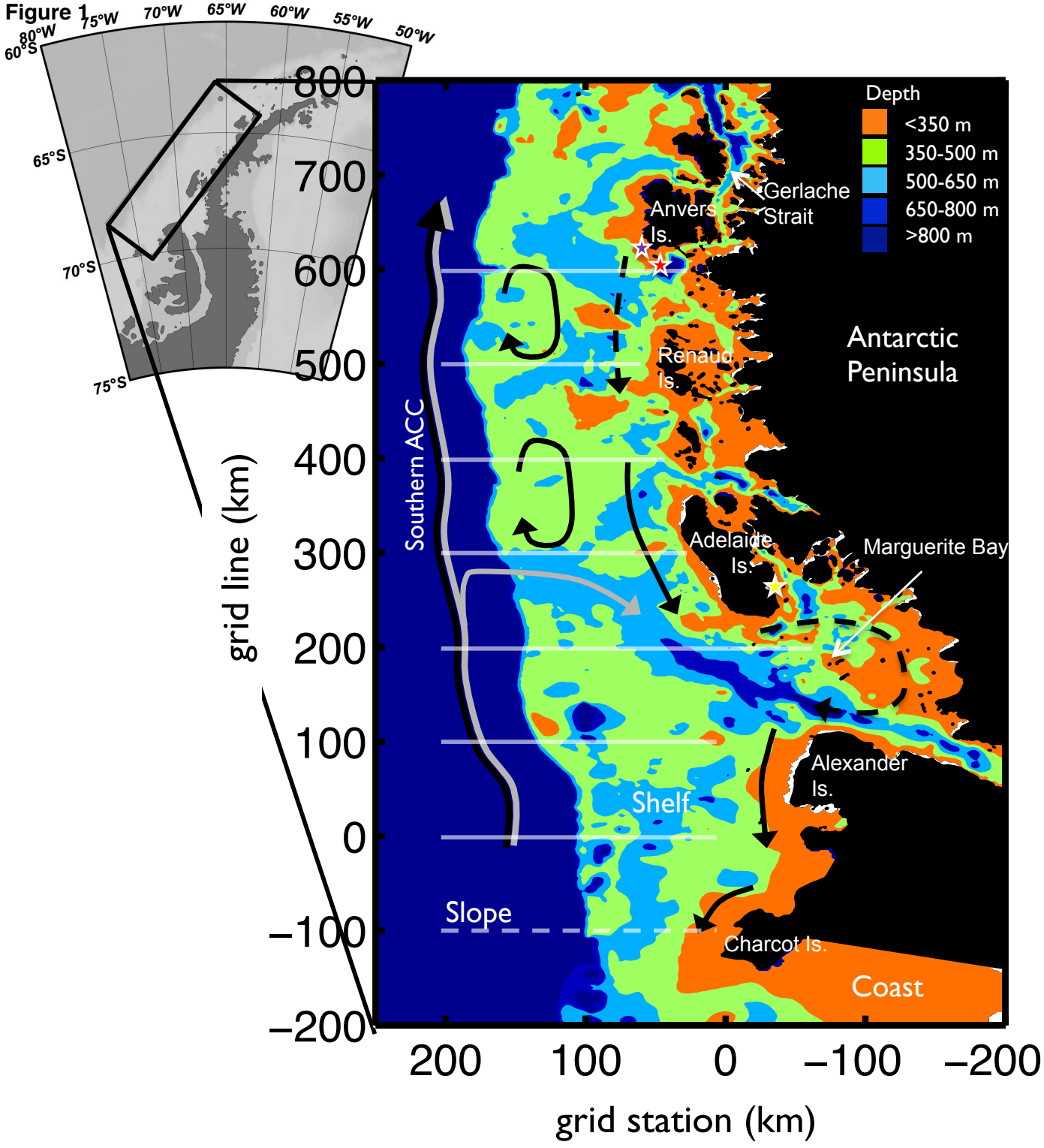
80°W
75°W
70°W
65°W
60°W
55°W
50°W
60°S
65°S
70°S
75°S
800
700
600
500
400
300
200
100
0
−100
−200
grid line (km)
200
100
0
−100
−200
grid station (km)
Depth
<350 m
350-500 m
500-650 m
650-800 m
>800 m
Gerlache Strait
Anvers Is.
Renaud Is.
Antarctic Peninsula
Southern ACC
Adelaide Is.
Marguerite Bay
Alexander Is.
Shelf
Slope
Charcot Is.
Coast

Figure 2

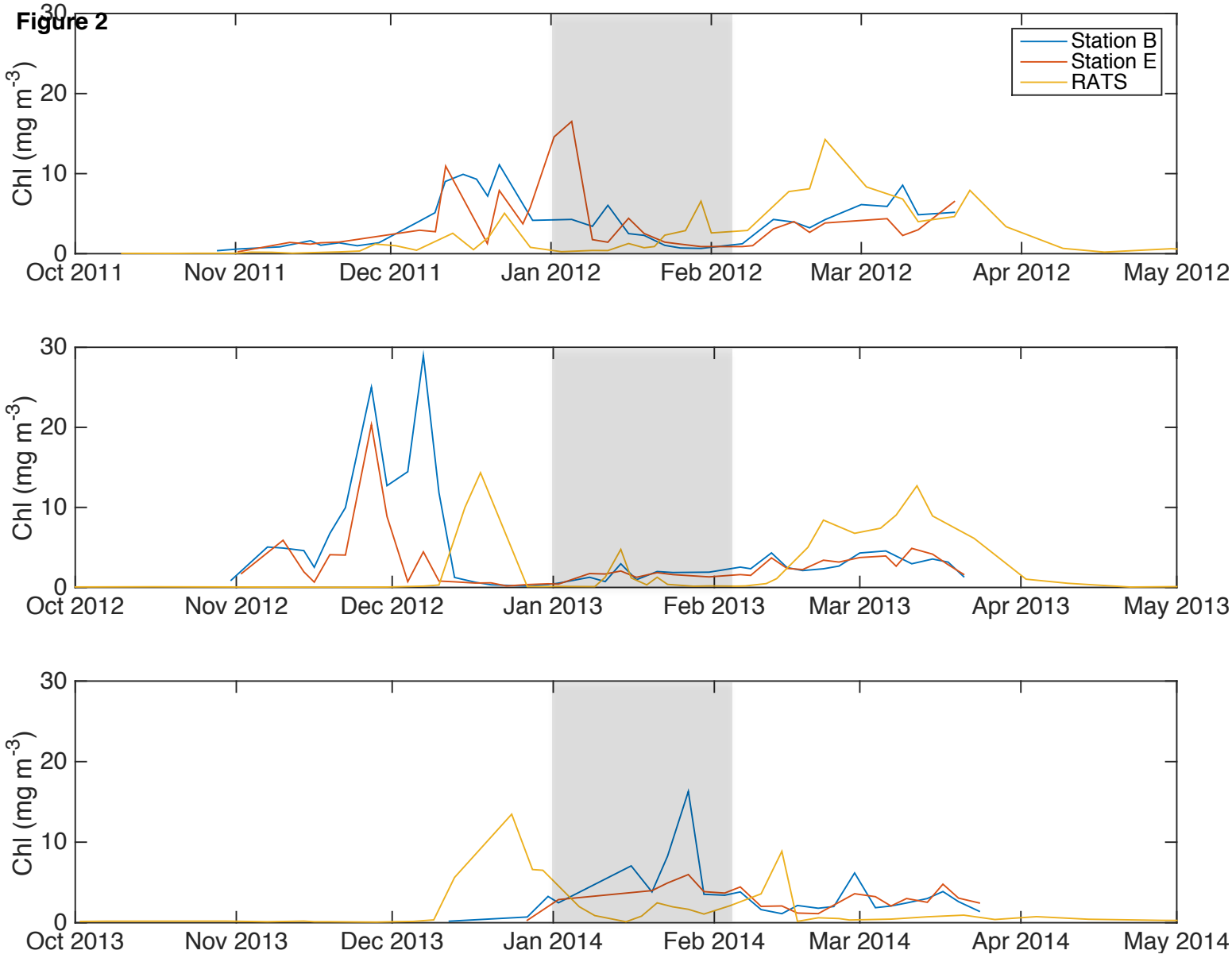
Station B
Station E
RATS
Chl (mg m-3)
0
10
20
30
Oct 2011
Nov 2011
Dec 2011
Jan 2012
Feb 2012
Mar 2012
Apr 2012
May 2012
Oct 2012
Nov 2012
Dec 2012
Jan 2013
Feb 2013
Mar 2013
Apr 2013
May 2013
Oct 2013
Nov 2013
Dec 2013
Jan 2014
Feb 2014
Mar 2014
Apr 2014
May 2014

Figure 3

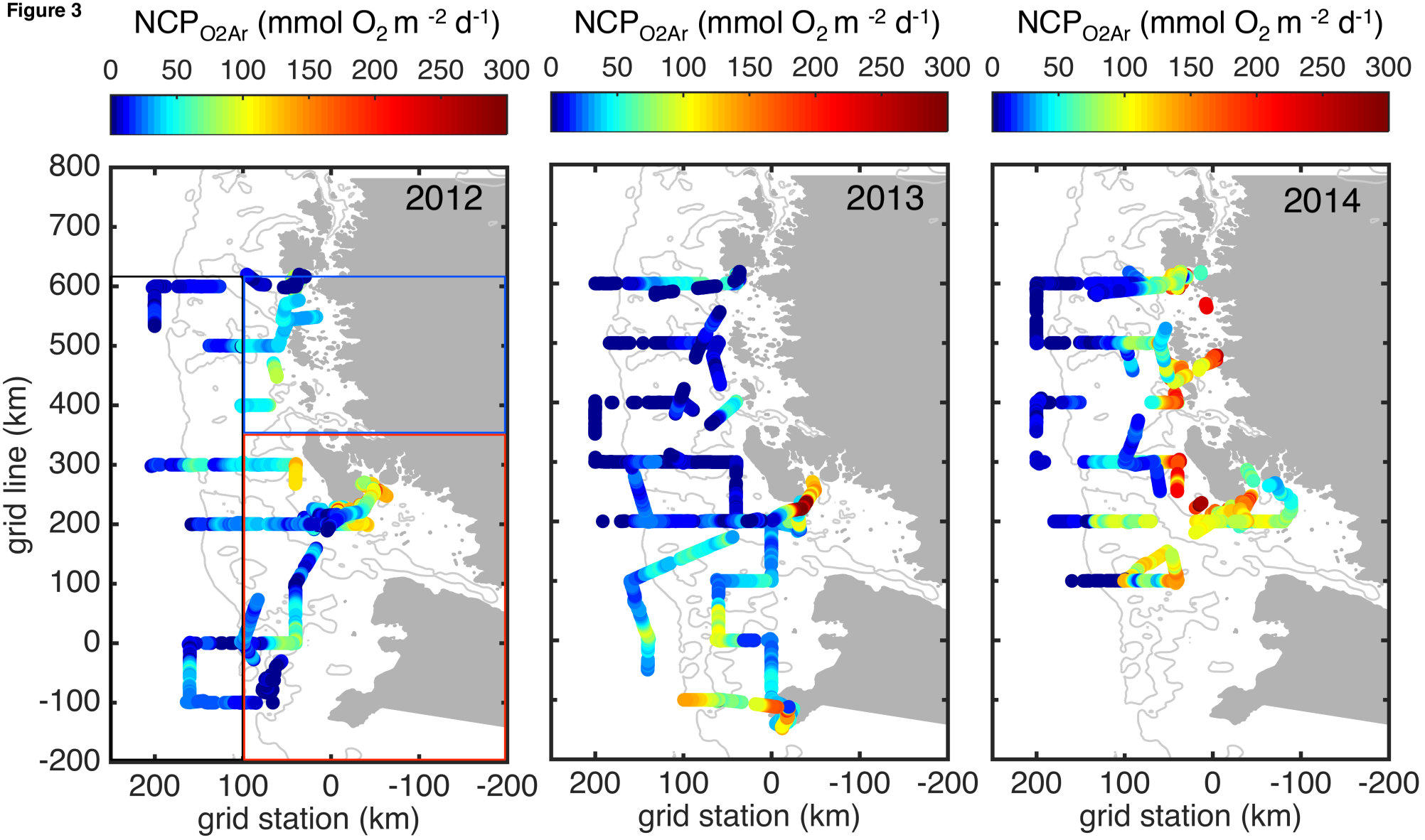
NCP$_{O2Ar}$ (mmol O$_2$ m^{-2} d^{-1})
0 50 100 150 200 250 300
2012
2013
2014
grid line (km)
800 700 600 500 400 300 200 100 0 -100 -200
grid station (km)
200 100 0 -100 -200

Figure 4

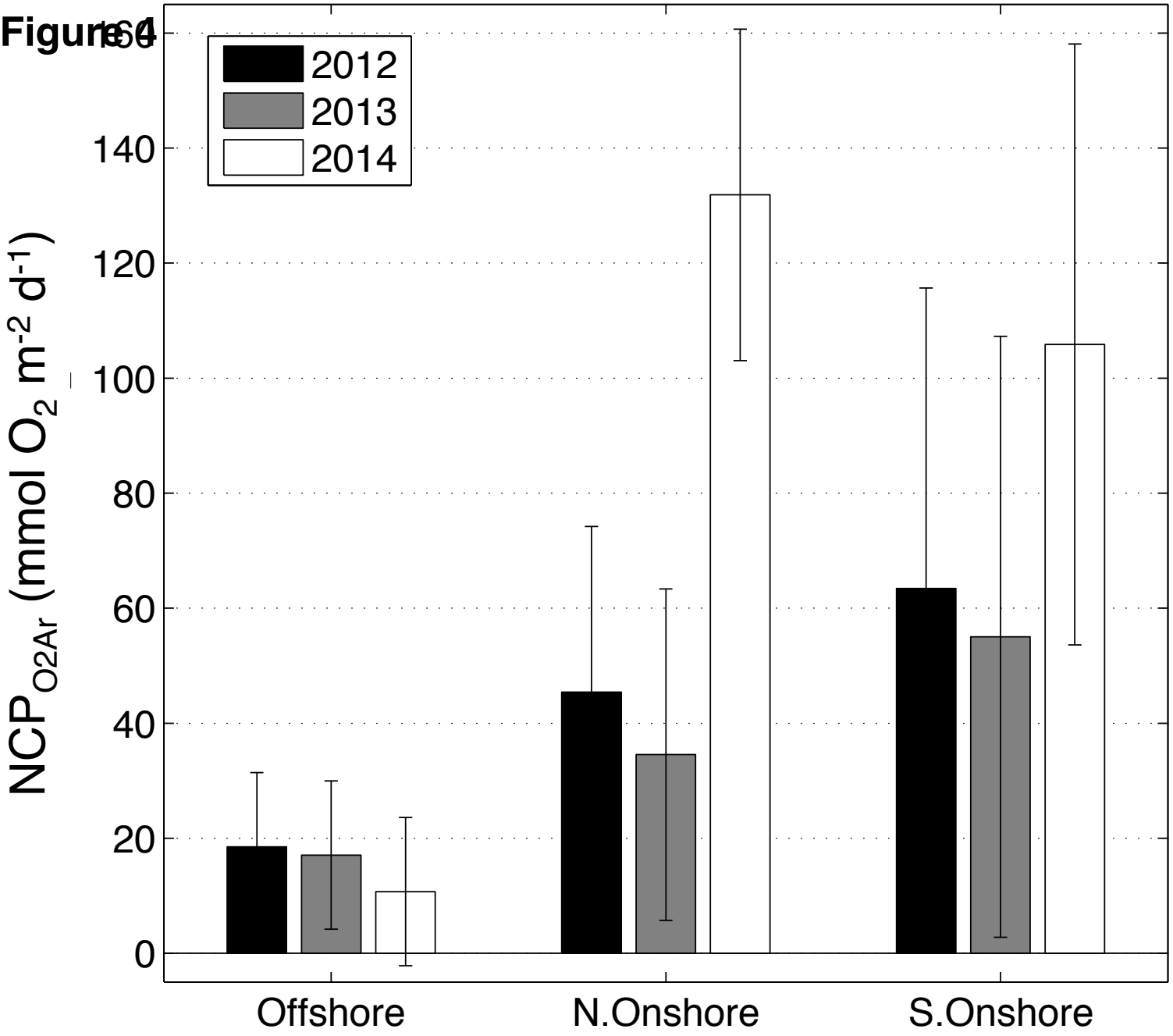
2012
2013
2014
160
140
120
100
80
60
40
20
0
NCP$_{O2Ar}$ (mmol O_2 m^{-2} d^{-1})
Offshore
N.Onshore
S.Onshore

Figure 5

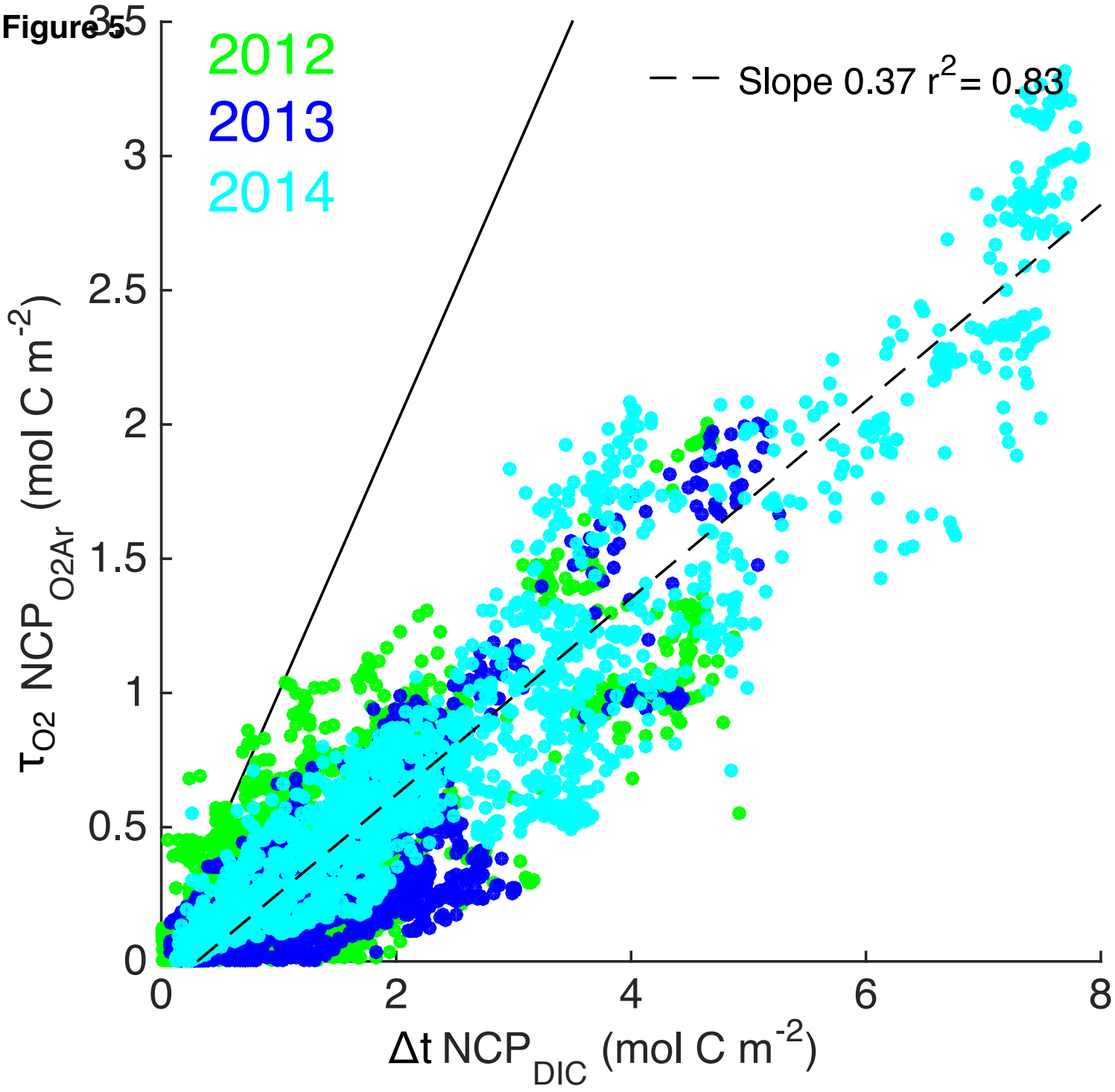
2012
2013
2014
Slope 0.37 r2= 0.83
τO2 NCPO2Ar (mol C m-2)
Δt NCPDIC (mol C m-2)
0
0.5
1
1.5
2
2.5
3
3.5
0
2
4
6
8

Figure 6

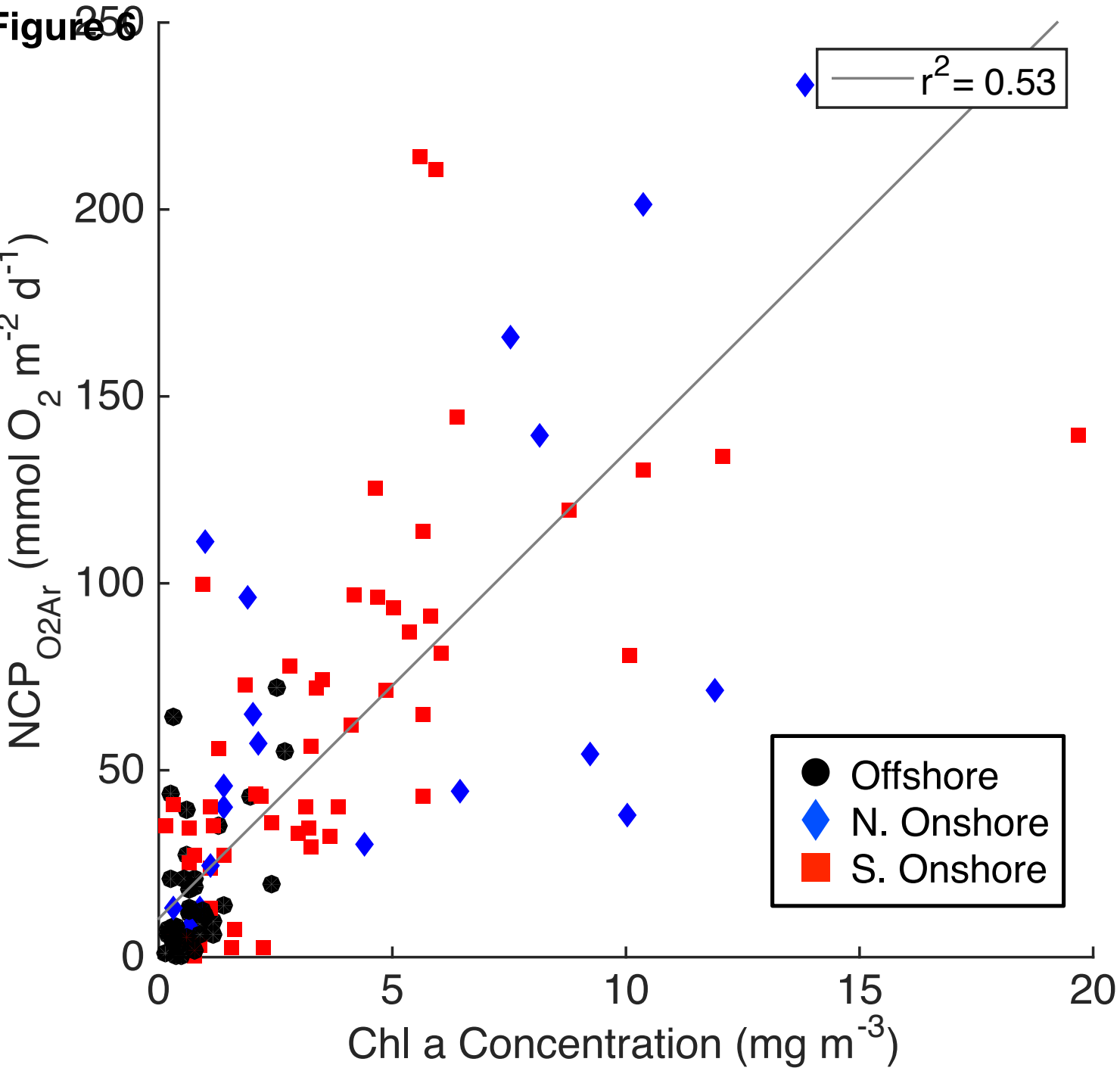
250
200
150
100
50
0
0
5
10
15
20
NCP O2Ar (mmol O2 m-2 d-1)
Chl a Concentration (mg m-3)
r2 = 0.53
Offshore
N. Onshore
S. Onshore

Figure 7

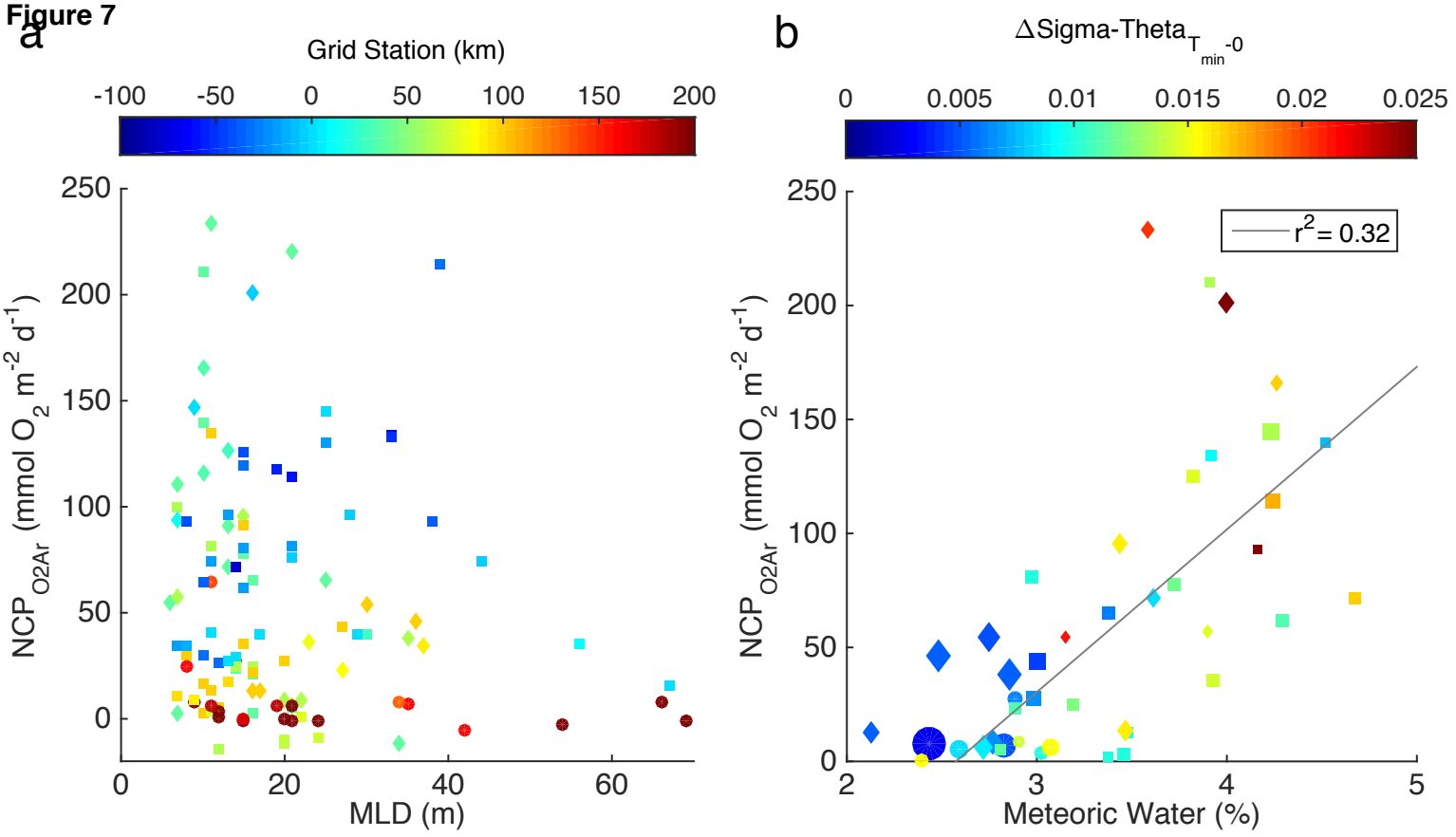
a
Grid Station (km)
-100
-50
0
50
100
150
200
250
200
150
100
50
0
NCP O2Ar (mmol O2 m-2 d-1)
0
20
40
60
MLD (m)
b
ΔSigma-Theta Tmin -0
0
0.005
0.01
0.015
0.02
0.025
r2 = 0.32
2
3
4
5
Meteoric Water (%)

Figure 8

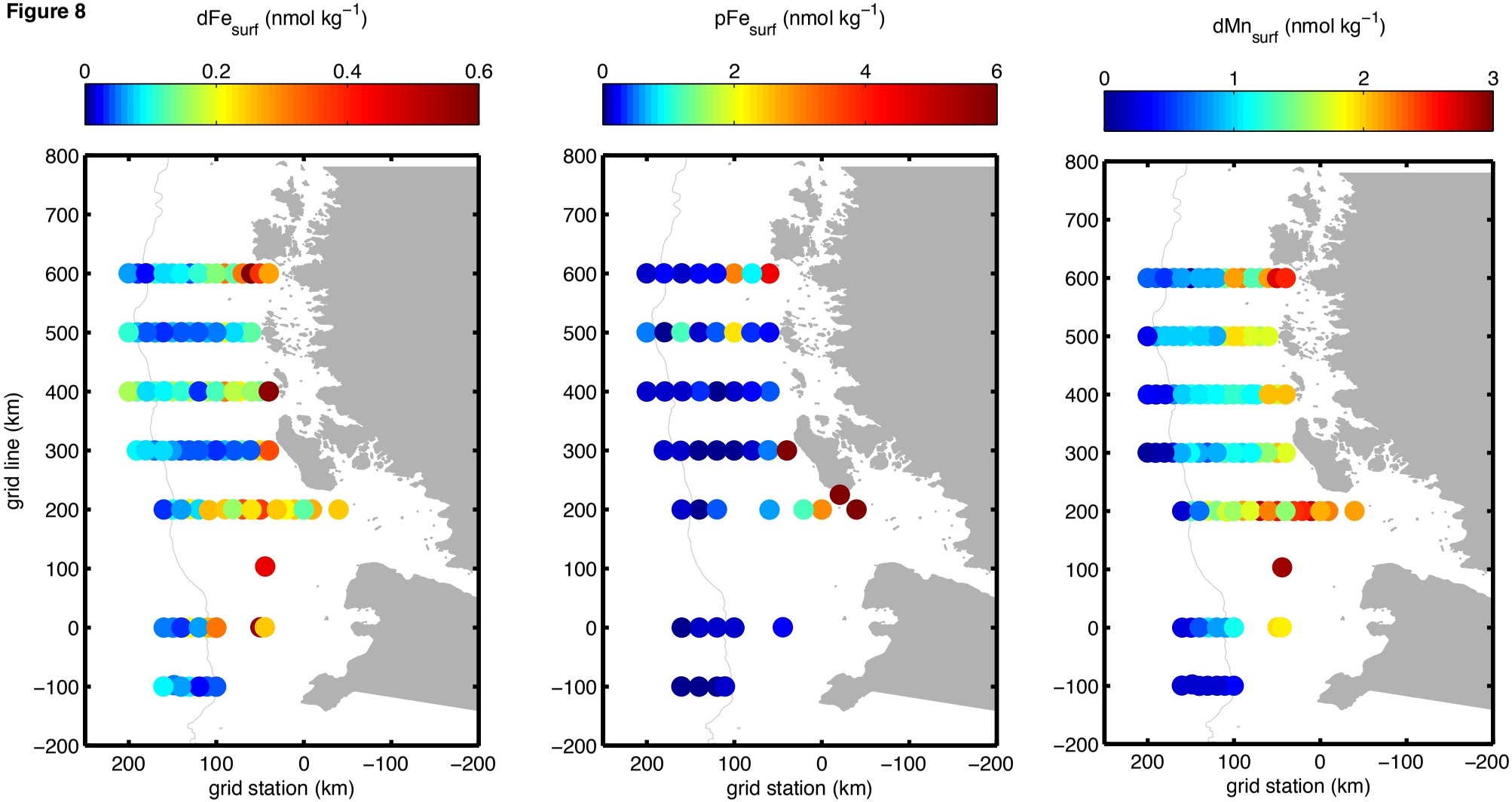
dFe surf (nmol kg−1)
0
0.2
0.4
0.6
pFe surf (nmol kg−1)
0
2
4
6
dMn surf (nmol kg−1)
0
1
2
3
grid line (km)
800
700
600
500
400
300
200
100
0
−100
−200
200
100
0
−100
−200
grid station (km)

Figure 9

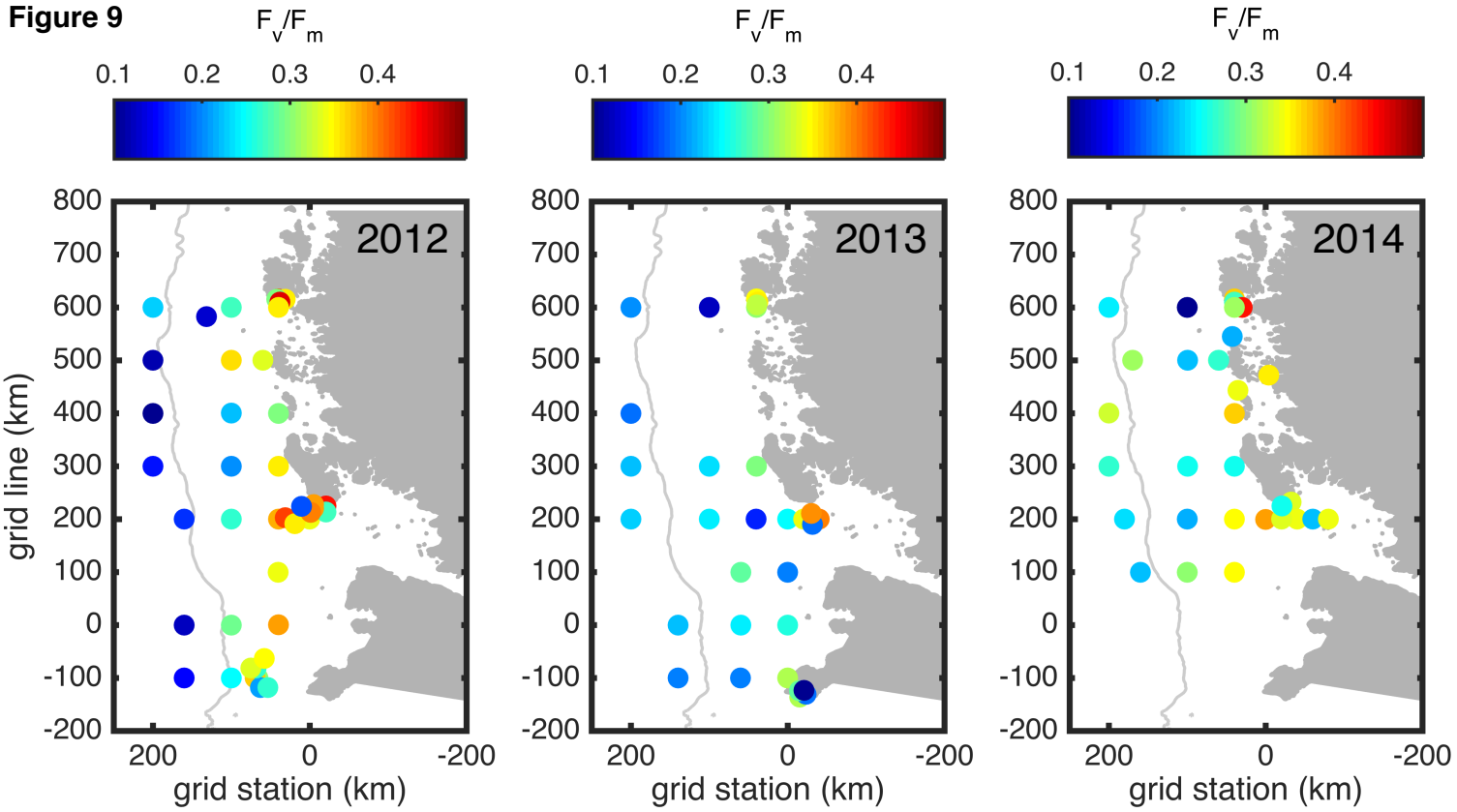
F v /F m
0.1 0.2 0.3 0.4
2012
2013
2014
grid line (km)
800 700 600 500 400 300 200 100 0 -100 -200
200 0 -200
grid station (km)

Figure 10

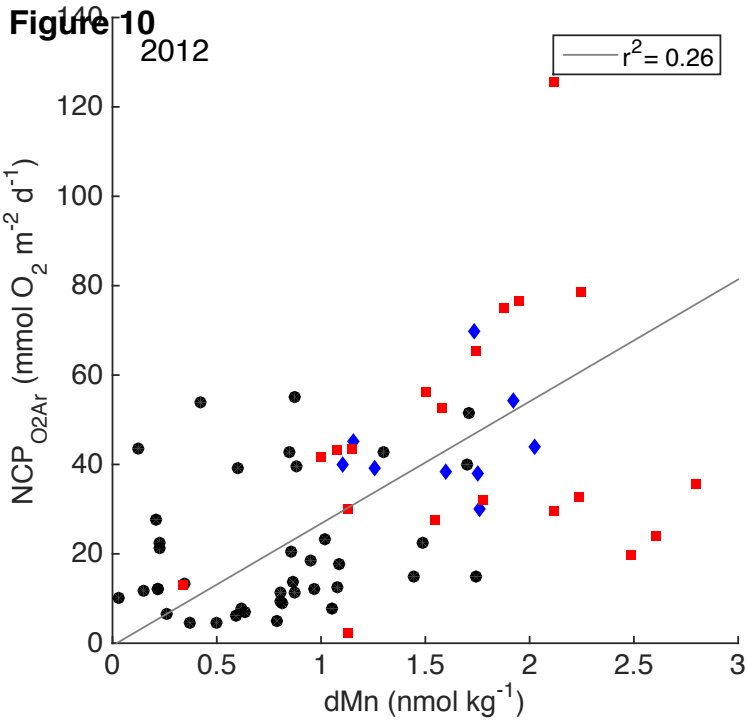
2012
r2= 0.26
NCP O2Ar (mmol O2 m-2 d-1)
dMn (nmol kg-1)

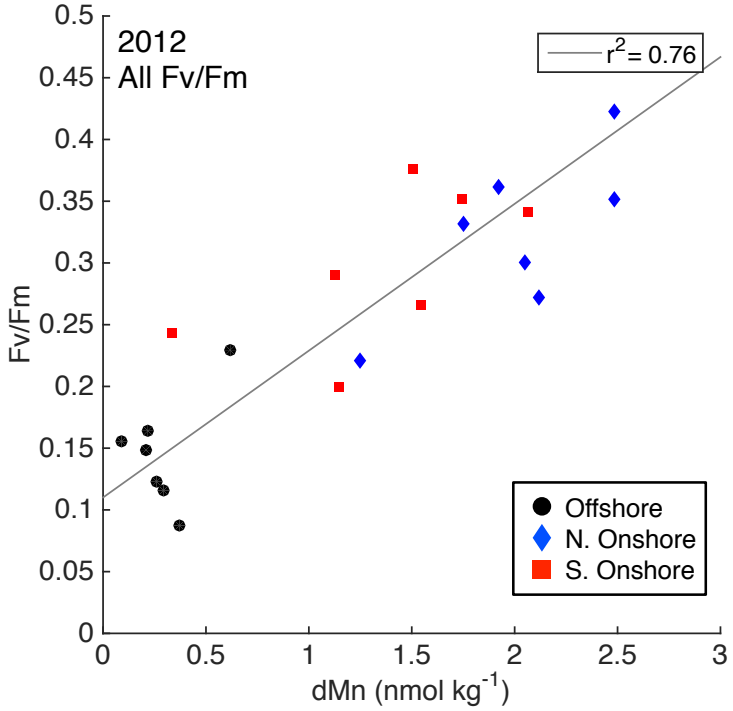
2012
All Fv/Fm
r2= 0.76
Fv/Fm
dMn (nmol kg-1)
Offshore
N. Onshore
S. Onshore

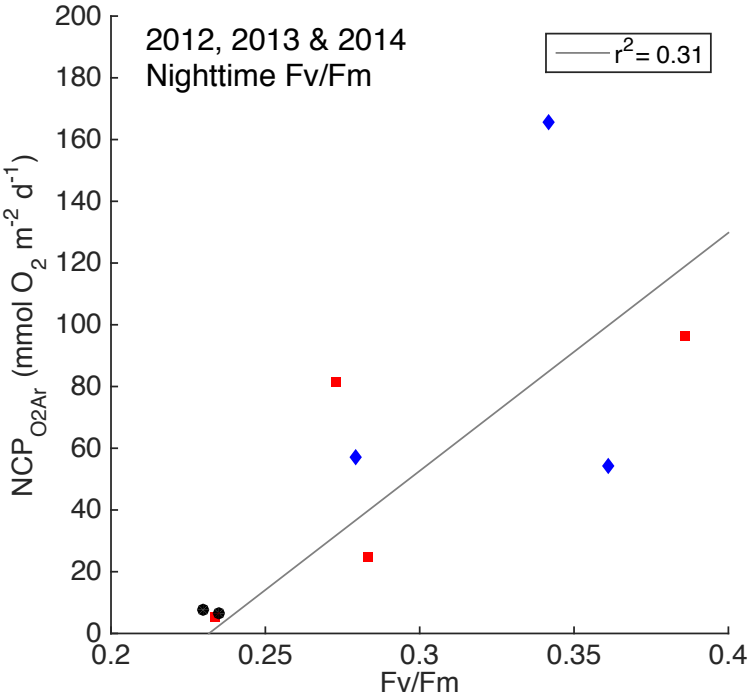
2012, 2013 & 2014
Nighttime Fv/Fm
r2= 0.31
NCP O2Ar (mmol O2 m-2 d-1)
Fv/Fm

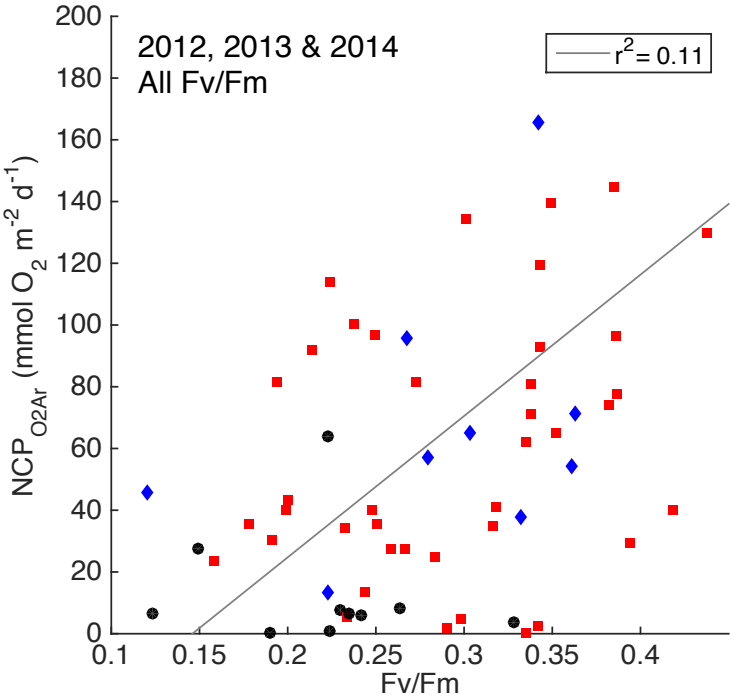
2012, 2013 & 2014
All Fv/Fm
r2= 0.11
NCP O2Ar (mmol O2 m-2 d-1)
Fv/Fm

Figure 11

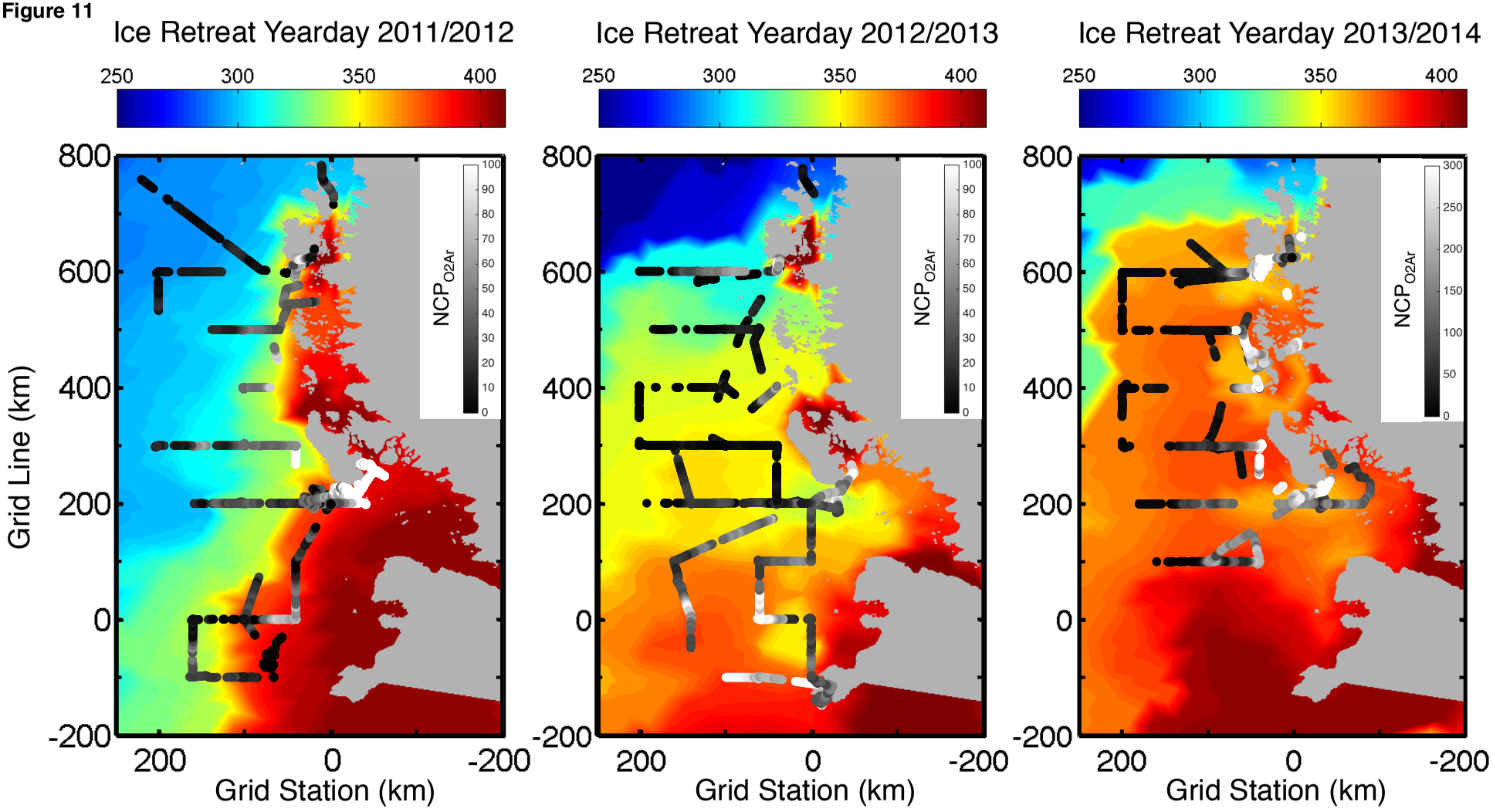
Ice Retreat Yearday 2011/2012
Ice Retreat Yearday 2012/2013
Ice Retreat Yearday 2013/2014
250
300
350
400
NCP O2Ar
Grid Line (km)
Grid Station (km)
800
600
400
200
0
-200